Cellular and Molecular Life Sciences (2023) 80:362
https://doi.org/10.1007/s00018-023-05021-1

ORIGINAL ARTICLE

Molecular basis of retinal remodeling in a zebrafish model of retinitis pigmentosa

Abirami Santhanam[1,2,5] · Eyad Shihabeddin[1,3] · Haichao Wei[4] · Jiaqian Wu[3,4] · John O'Brien[1,2,3]

Received: 22 July 2023 / Revised: 10 October 2023 / Accepted: 27 October 2023 / Published online: 18 November 2023

Abstract

A hallmark of inherited retinal degenerative diseases such as retinitis pigmentosa (RP) is progressive structural and functional remodeling of the remaining retinal cells as photoreceptors degenerate. Extensive remodeling of the retina stands as a barrier for the successful implementation of strategies to restore vision. To understand the molecular basis of remodeling, we performed analyses of single-cell transcriptome data from adult zebrafish retina of wild type AB strain (WT) and a P23H mutant rhodopsin transgenic model of RP with continuous degeneration and regeneration. Retinas from both female and male fish were pooled to generate each library, combining data from both sexes. We provide a benchmark atlas of retinal cell type transcriptomes in zebrafish and insight into how each retinal cell type is affected in the P23H model. Oxidative stress is found throughout the retina, with increases in reliance on oxidative metabolism and glycolysis in the affected rods as well as cones, bipolar cells, and retinal ganglion cells. There is also transcriptional evidence for widespread synaptic remodeling and enhancement of glutamatergic transmission in the inner retina. Notably, changes in circadian rhythm regulation are detected in cones, bipolar cells, and retinal pigmented epithelium. We also identify the transcriptomic signatures of retinal progenitor cells and newly formed rods essential for the regenerative process. This comprehensive transcriptomic analysis provides a molecular road map to understand how the retina remodels in the context of chronic retinal degeneration with ongoing regeneration.

Keywords Retinitis pigmentosa · Retinal degeneration · Regeneration · Photoreceptor · Pigmented epithelium · Synapse remodeling · Oxidative metabolism

Introduction

Retinitis pigmentosa (RP) is a debilitating, genetically based disease that affects 1 in 4000 people worldwide [1, 2]. Early symptoms of RP include loss of peripheral and night vision due to the death of rod photoreceptors [3], generally progressing to complete blindness due to the death of cone photoreceptors via a bystander effect [4, 5]. With loss of vision beginning in young adults, some patients are completely blind by their early thirties [6]. Gene therapy for one variant of RP has been somewhat effective [7], but due to the large number of genes that can cause RP [8], there are no treatment options for most patients. Regenerative medicine and stem cell transplantation offer significant hope to combat the progression to blindness and preserve vision [9, 10].

A notable barrier to implementing regenerative and transplantation strategies is the extensive remodeling of retinal cell types that are not themselves directly affected by the mutations that cause degeneration [11]. This remodeling

Abirami Santhanam and Eyad Shihabeddin contributed equally.

✉ Abirami Santhanam
abirami.santhanam@bcm.edu

✉ John O'Brien
jobrien3@Central.UH.EDU

1 Department of Ophthalmology & Visual Science, McGovern Medical School, The University of Texas Health Science Center at Houston, Houston, TX 77030, USA

2 University of Houston College of Optometry, Houston, TX 77204, USA

3 MD Anderson UT Health Graduate School of Biomedical Sciences, Houston, TX 77030, USA

4 Department of Neurosurgery, McGovern Medical School, The University of Texas Health Science Center at Houston, Houston, TX 77030, USA

5 Present Address: Human Genome Sequencing Center, Baylor College of Medicine, Houston, TX 77030, USA

entails extensive alterations of Müller glial cells and retinal pigmented epithelium (RPE), as well as development of ectopic synapses among neurons [12–17]. Along with remodeling comes aberrant spontaneous neuronal activity, obscuring the transmission of visual signals [18–21]. Understanding the molecular underpinnings of this remodeling and aberrant activity will be paramount to developing successful strategies to regenerate retina and restore functional retinal circuitry.

The revolution in large-scale genomic and transcriptomic methods has revealed the transcriptional diversity of cell types with unprecedented detail. These techniques have been used to resolve cell type complexity in the retina [22, 23] and to examine development [24]. Recent studies have revealed the retinal response to acute injury, including the transcriptional changes that support the regeneration of neurons from Müller glial precursors [25]. However, these studies lack the context of retinal remodeling found in chronic retinal degenerative diseases such as RP. We have previously characterized a transgenic zebrafish line expressing P23H mutant rhodopsin, which models the most common form of autosomal dominant retinitis pigmentosa with ongoing photoreceptor degeneration and regeneration [26]. In the present study, we have performed single-cell RNA sequencing (sc-RNA Seq) of adult retina to assess the transcriptomic remodeling that takes place in the P23H zebrafish model. In addition to providing a benchmark atlas of retinal cell type transcriptomes in the WT adult zebrafish retina, we find transcriptional changes in essentially all cell types, reflective of the remodeling that has gone on in the chronic disease. Prominent changes reveal pathology in RPE structural integrity, synaptic remodeling in several cell types, and disruption in circadian clock gene expression. We have further identified the retinal progenitor cell population differentiating into rod photoreceptors. Collectively, our results provide a comprehensive understanding of the transcriptomic changes that take place throughout the retina in a model with chronic retinal degeneration. Ultimately, this will allow for therapeutic approaches to compensate for remodeling that otherwise limits their efficacy.

Materials and methods

Animal husbandry

Rearing, breeding, and staging of zebrafish (*Danio rerio)* were performed following standard procedures in the zebrafish community [27]. AB strain WT zebrafish were purchased from the Zebrafish International Resource Center (ZIRC; Eugene, OR, USA; RRID: ZIRC_ZL1), raised, bred, and maintained on a 14 h light/10 h dark cycle. P23H rhodopsin transgenic zebrafish (ZFIN name uth4Tg; ID ZDB-ALT-210330-3) were developed in-house and characterized in a previous publication [26]. Randomly selected fish between 6 and 10 months of age were used for all experiments. All procedures employing animals comply with the U.S. Public Health Service policy on humane care and use of laboratory animals and the NRC Guide for the Care and Use of Laboratory Animals and have been reviewed and approved by the Institutional Animal Care and Use Committee at the University of Texas Health Science Center at Houston under protocols HSC-AWC-15-0057 and HSC-AWC-18-0047, and at the University of Houston under protocol PROTO202100037.

Zebrafish retinal dissociation and single-cell cDNA library preparation

For each sample submitted for single-cell RNA sequencing (sc-RNA Seq), 3 fish of the same strain were collected in the morning between nine and eleven a.m., 1 to 3 h after light onset in the fish room, in Falcon tubes containing 0.15% Tricaine/MS222 and incubated on ice for 10 min. Zebrafish were decapitated and eyeballs were detached and placed in dissecting medium containing Leibovitz's L-15 medium (Gibco 21083027). Each retina, along with adherent patches of retinal pigmented epithelium (RPE), was then extracted and placed in a 1.5 mL micro-centrifuge tube with 300 µL of dissociation solution containing L15 and Earle's Balanced Salt Solution (EBSS; Gibco 14155063) in a 3:1 ratio. After all retinas were collected, the dissociation solution was replaced with 200 µL of Papain solution (50 U/mL in EBSS; Worthington Biochemical LK003178) and retinas were incubated at 28 °C. After 20 min of incubation, retinas were gently triturated 20–30 times with fire-polished glass pipettes. Supernatants were collected and incubated with Papain for another 40 min with trituration performed every 10 min. Papain reaction was terminated by adding 2 × volume of 0.1% BSA in L15: EBSS medium. Tubes were centrifuged at 400 g for 5 min to pellet the cells. The supernatant was removed and washed again with 0.05% BSA in L15: EBSS. The supernatant was removed and cells were finally suspended in 100 µl of 0.05% BSA in L15: EBSS. Cells were checked for cell viability and counted to get a final concentration of at least ~ 800 to 1000 cells/µl.

The cell samples were submitted for 3′ sc-RNA library preparation and sequencing through the Baylor College of Medicine Single Cell Genomics Core facility. Single-cell Gene Expression Libraries were prepared using Chromium Next GEM Single Cell 3′ Reagent Kits v2 and v3.1 (10 × Genomics, Pleasanton, CA). In brief, single cells, reverse transcription (RT) reagents, Gel Beads containing barcoded oligonucleotides, and oil were loaded on a Chromium controller (10 × Genomics) to generate single-cell GEMS (Gel Beads-In-Emulsions) where full-length cDNA

was synthesized and barcoded for each single cell. Subsequently, the GEMS were broken and cDNA from every single cell pooled. Following cleanup using Dynabeads MyOne Silane Beads, cDNA was amplified by PCR. The amplified product was fragmented to optimal size before end-repair, A-tailing and adaptor ligation. cDNA libraries were sequenced on an Illumina HiSeq2500.

Single-cell RNA seq data analysis

Sequences were run through the 10 × Genomics CellRanger V3.1.2.0 pipeline. First, sequences were demultiplexed into FASTQ files through CellRanger mkfastq. FASTQ files were then aligned to the Zf reference genome (GCA_000002035.4_GRCz11) through CellRanger count. Output files were run through Babraham Bioinformatics' FASTQC V0.11.9 to check on the quality of the sequences used for analysis. Sequences had a normal distribution of GC content as well as base call accuracy above 99%. Over 93% of reads mapped successfully to the genome. Computational analysis was performed through Texas Advanced Computing Center (TACC) Lonestar5 computing service. Scripts were written in Notepad + + v7.6.2 and uploaded to TACC through PuTTY V0.72.

The total number of DNA sequence reads for v3.1 datasets was 608,597,236 for P23H and 967,526,548 for WT. All reads were aligned to the Zf reference genome (GCF_000002035.6_GRCz11) through Texas Advanced Computing Center's (TACC's) Lonestar5 computing system. After alignment, quality control was assessed through FASTQC. Aligned data were run through the Seurat V3.1.1 package [28] in R V3.6.1. Cells initially reported for analysis were 15,585 for P23H and 13,966 for WT datasets. From a total of 15,585 cells (P23H), we obtained an average of 39,050 reads per cell and median of 1241 UMIs (unique transcripts) per cell. We detected a total of 26,375 genes from the P23H dataset. From a total of 13,966 cells (WT), we obtained an average of 69,277 reads per cell and median of 1198 UMIs per cell. We detected a total of 25,673 genes from the WT dataset. The reported median genes per cell for P23H and WT datasets were 684 and 658 genes, respectively.

In the Seurat processing, any cell that was determined to be an outlier or contained greater than 10% mitochondrial genes was removed. Low-abundant genes (expressed in fewer than 10 cells) and cells of potentially low quality (percentage of mitochondrial genes > 10%) were removed from downstream analysis. P23H and WT datasets contained between 200 and 4700 genes and 200 and 6000 genes per cell, respectively (Table S4). PCElbowPlots were performed, and 20 principal components were used for downstream analysis of each dataset. PC1 to PC20 were used to construct nearest neighbor graphs in the PCA space followed by Louvain clustering and non-linear dimensional reduction by tSNE to visualize and explore the clusters. Each cluster was assigned a cell type based on their expression of cell type-specific marker genes (Table S1). Dot plots, Heatmaps, Violin Plots, and tSNE cluster maps were all generated through Seurat's vignettes V3.2. Expression levels are expressed in a base 2 log scale. Statistical significance between expression levels was determined using Wilcoxon 'Mann–Whitney' test (two-sided, unpaired with 95% confidence level).

Network analysis

Differentially expressed genes (DEGs) for each cluster were imported into Cytoscape's plugin ClueGo 3.9.0 [29] (https://cytoscape.org/) to visualize the non-redundant biological networks involved for each cluster. Pathways that show a p value less than 0.05 were used for analysis. Networks were assessed to determine the functional roles and differences between the P23H and WT datasets. We also used the tool Metascape [30] (https://metascape.org/) for a comprehensive analysis of the differentially expressed genes (DEGs) from different cell types. Functional Enrichment Analysis to determine protein–protein interaction networks was performed on genes of interest through STRING V11.0 (https://string-db.org/).

Fluorescent in-situ hybridization multiplex/HiPlex

All fish for tissue analysis were collected during the morning between nine and eleven a.m. and anesthetized in 0.15% of Tricaine/MS222 on ice. Fish were then decapitated and eyeballs enucleated and fixed in 4% formaldehyde (PFA) in 0.1 M phosphate buffer (PB), pH 7.5 for 24 h at RT. Eyes were then washed four times at 15-min intervals in PB and cryo-protected in 30% sucrose in PB overnight at 4 °C. Eyes were then frozen in Tissue-Tek O.C.T. compound (Sakura Finetek, Torrance, CA, USA) using dry ice and stored at −80 °C. Retinal sections were cut at 20 µm on a cryostat (Leica) and stored at − 80 °C until use. We used the RNAscope Hiplex detection reagents supplied by the manufacturer (Advanced Cell Diagnostics, Newark, CA, USA) along with the specific probes for target genes. HiPlex and subsequent fluorescent multiplex assays were performed following the manufacturer's instructions [31]. Briefly, sections were fixed in 4% PFA, dehydrated with 50%, 70%, and 100% ethanol, then treated with protease (from the HiPlex kit 324419). In HiPlex, all gene targets are hybridized and amplified together, whereas detection is achieved iteratively in groups of 2–3 targets. Sections were incubated with pooled HiPlex probes and amplified with a series of amplification solutions, then a detection solution was applied. Samples were hybridized with probes

and incubated with amplification solution; signals were visualized by applying detection solution. Cell nuclei were counterstained with DAPI and samples were mounted. Images were taken using a Zeiss LSM 800 laser scanning confocal microscope. After each round, samples were treated with TCEP solution to cleave fluorophores (from the HiPlex kit 324419), then moved on to the next round of the fluorophore detection procedures.

Immunohistochemistry

Immunohistochemistry (IHC) was performed in the same manner as in our previously published work [26]. Retinas were fixed in 4% PFA for 1 h, embedded and sectioned with a cryostat as described for in situ hybridization. Sections were used for immunohistochemistry by incubation in (i) blocking solution 5% Donkey Serum (Jackson ImmunoResearch; West Grove, PA) in PBS (P3813, Millipore-Sigma, St. Louis, MO) with 0.3% Triton X-100 for 1 h at room temperature; (ii) primary antibody diluted in PBS, 0.1% Triton X-100 and 5% serum overnight at room temperature; (iii) fluorescent secondary antibody (Jackson ImmunoResearch), diluted as the primary antibody, for 1 h at room temperature. For nuclear counterstaining, retinal sections were mounted in Vectashield with DAPI (H-1000; Vector Laboratories; Burlingame, CA) and cover-slipped. ZO-1 Antibody (Cat. # 33-9100, RRID: AB_2533147, Thermo Fisher Scientific) was diluted 1:100 for IHC.

Results

Single-cell transcriptomic atlas of zebrafish retina

To establish a benchmark from which to understand changes associated with retinal degeneration, we first developed a cell atlas of the WT adult zebrafish retina using single-cell 3′ RNA sequencing (scRNA-seq). The single-cell library was derived from pooled cells from retinas of three WT fish, two females and one male, at the age of 7 months. The library was developed using the 10X Genomics Chromium platform. We have repeated the experiments twice with different single-cell chemistries V2 and V3. Both runs provided similar cluster patterns and cell types. The data presented here are from the V3 chemistry as this has improved Median Genes per Cell and Median UMI Counts (unique transcripts) per Cell. Following quality control and filtering using the Seurat (V3) package [28], the final dataset contained 13,552 cells. The scRNA-seq data were initially analyzed using an unsupervised graph clustering approach implemented in Seurat to classify individual cells into cell populations according to similarities in their transcriptome profiles. Figure 1A shows a tSNE plot visualization of the clusters in two-dimensional space. Overall, the cells were classified into 23 transcriptionally distinct clusters.

The clusters were classified into different retinal cell types using markers identified in previous studies (Table S1). We were not able to assign any cellular identity to one cluster as it expressed markers from multiple retinal cell types. This cluster is not shown in the figure and was not used for further analysis. All the major retinal cell types are represented, including five clusters of amacrine cells, three clusters of microglia, two clusters each of cones, bipolar cells, retinal pigmented epithelium (RPE) and Müller glia, and one cluster each of rods, horizontal cells, retinal ganglion cells, neurogenic progenitor cells (NPCs), oligodendrocytes and retinal progenitor cells (RPCs). Each cell type cluster expresses a unique set of genes along with some genes shared between clusters that define it as a specific cell type. The top 5 genes that are specifically enriched in each cell type are displayed in the heatmap shown in Fig. 1B; a list of the top 10 genes in each cluster is listed in Table S2.

Cellular changes in a zebrafish model of retinitis pigmentosa

To identify transcriptional changes that occur during chronic retinal degeneration and regeneration, we performed the same type of analysis on a single-cell transcriptome library prepared from the adult retina of a transgenic zebrafish model of retinitis pigmentosa expressing P23H mutant rhodopsin [26]. Following quality control and filtering, our final dataset contained 15,511 cells. We compared the WT and P23H datasets using an integration algorithm, which aims to identify shared cell states that are present across different datasets (Fig. 2A). Using the integrated analysis, we detected all the major cell types that are present in the WT dataset, but there were differences in the number of cells in different cell types (Fig. 2A, B). There was a reduction in the number of mature rod photoreceptors (cluster 3) in the P23H retina, reflecting the ongoing degeneration occurring in this model system. In addition, a class of newly differentiated rods (cluster 13) that shows both progenitor and rod markers that did not appear in the clustering of the WT dataset was present. While some cells from the WT retina fell into this cluster, this class was threefold more abundant in the P23H retina, reflecting the continuous regeneration underway in the P23H retina (Fig. 2B, C). In keeping with this, we also detected a fourfold higher number of retinal progenitor cells (RPCs) in the P23H retina compared to the WT (Fig. 2C, cluster 14). Interestingly we saw an eightfold decrease in retinal pigmented epithelial cells (RPE, clusters 10 and 15) compared to WT (Fig. 2C).

Numerical comparisons of cell numbers in single-cell transcriptome data present challenges for interpretation. Cells of different types are not captured with equal efficacy

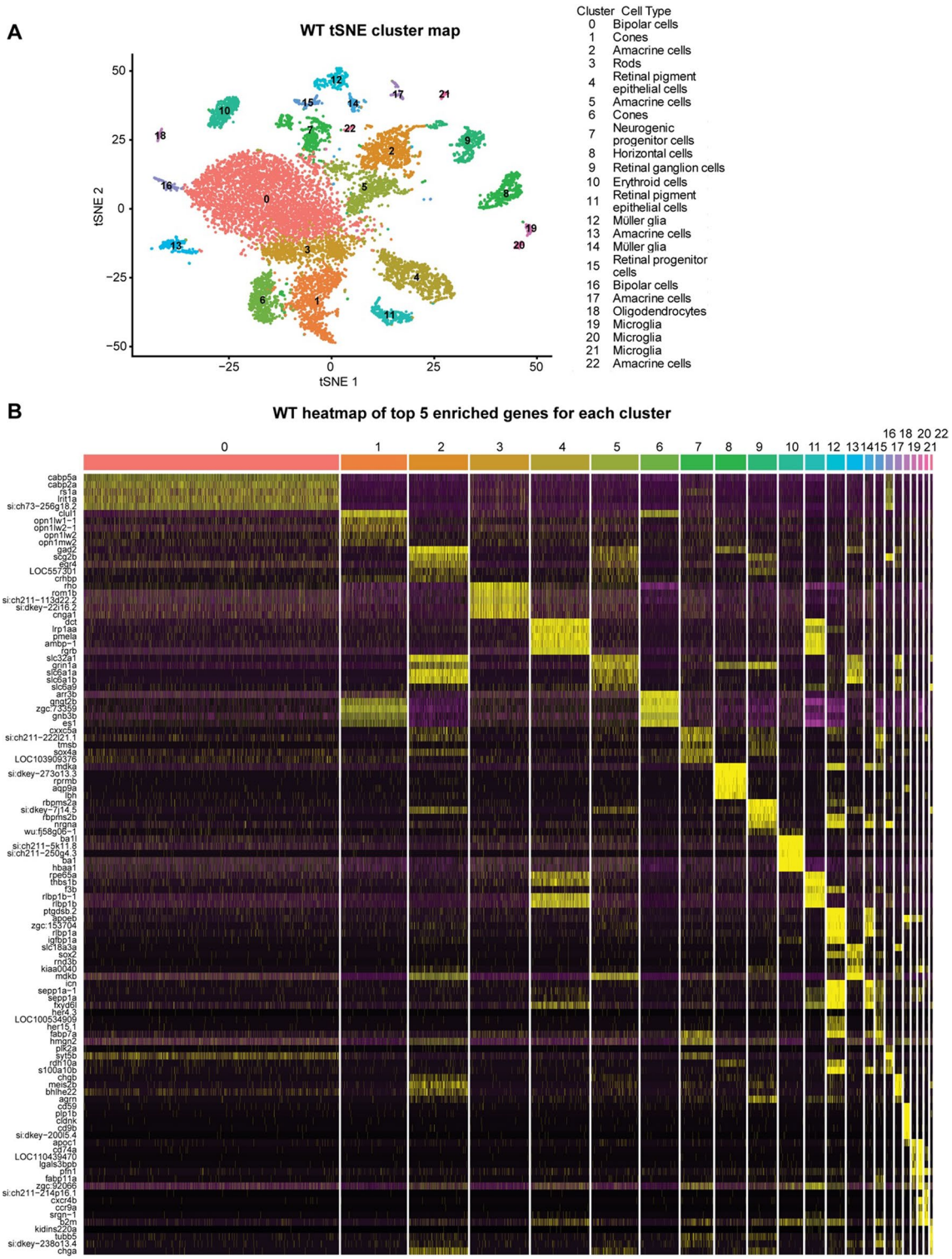

Fig. 1 Single-cell RNA seq analysis of WT zebrafish retina. **A** tSNE dimensionality reduction and visualization of transcriptional profiles of 13,552 retinal cells from WT zebrafish. **B** Heatmap showing the top 5 genes enriched for each cluster

and tissue dissociation conditions can favor the preservation of some cell types and the loss of others (e.g., the larger number of bipolar cells than photoreceptors in our datasets). To reinforce the estimates of relative changes in the numbers of cells of certain types, we also examined the numbers of cells in an earlier dataset using 10 × V2 chemistry prepared

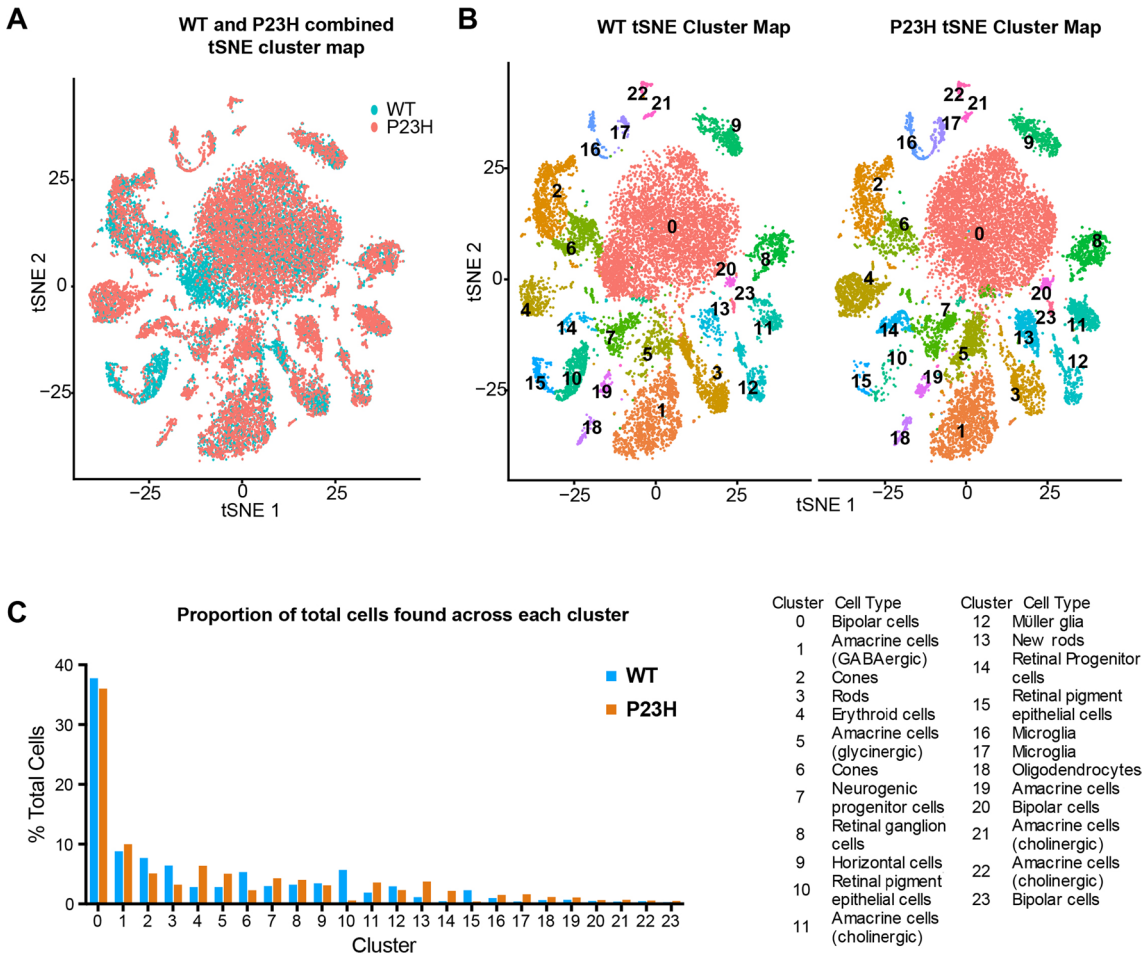

Fig. 2 Single-cell RNA seq analysis of integrated WT-P23H zebrafish retina datasets. **A** Overlap of tSNE dimensionality reduction and visualization of single-cell transcriptomes from WT and P23H transgenic fish retina. **B** Separate display of P23H and WT tSNE maps from integrated data set with cell types labeled. **C** Relative proportions of each cell type found in the P23H and WT retinal samples

using different animals of comparable age. Table S3 shows that trends in the relative ratios of cell numbers are conserved between datasets. In this dataset, we find that rods are more than twofold reduced in the P23H, whereas the newly formed rods are ninefold higher in P23H. Our dataset from V2 chemistry also showed a reduction of RPE cells in P23H compared to the WT (2.7-fold decrease in P23H) (Table S3).

Rod photoreceptors display enhanced oxidative metabolism, oxidative stress, and synaptic remodeling

Our previous study showed that rod photoreceptors undergo continuous cell death and that the number of rods is almost fourfold less in the P23H retina than in the WT [26]. Our current single-cell study also reflects the decrease in the number of rods in the P23H dataset compared to the WT (Fig. 3A). Violin plots of the expression of individual genes in a cluster allow us to compare gene expression levels in P23H and WT conditions. Figure 3B shows violin plots of the rod dominant genes rhodopsin (*rho*) and rod arrestins (*saga* and *sagb*). The expression of all of these genes was conserved between WT and P23H. We performed functional pathway analysis using Cytoscope Cluego [29] and Metascape [30] analysis software (Fig. S1). The P23H rod dataset revealed an increased level of markers for oxidative stress (*sirt2*, *atf4a*, and *oxr1b*), response to misfolded proteins (*hsp70.3*, *hspa5*, *dnajb1b*, and *xbp1*), actin de-polymerization (*eps8* and *sptbn1*) (Fig. 3C), and lipid phosphorylation (*dgkzb*, *pik3ca*, and *pik3r3a*) (Fig. 3D), reflecting physiologic responses to the P23H mutant rhodopsin that ultimately lead to photoreceptor degeneration. Interestingly we have also seen the increased transcriptome of certain ciliary

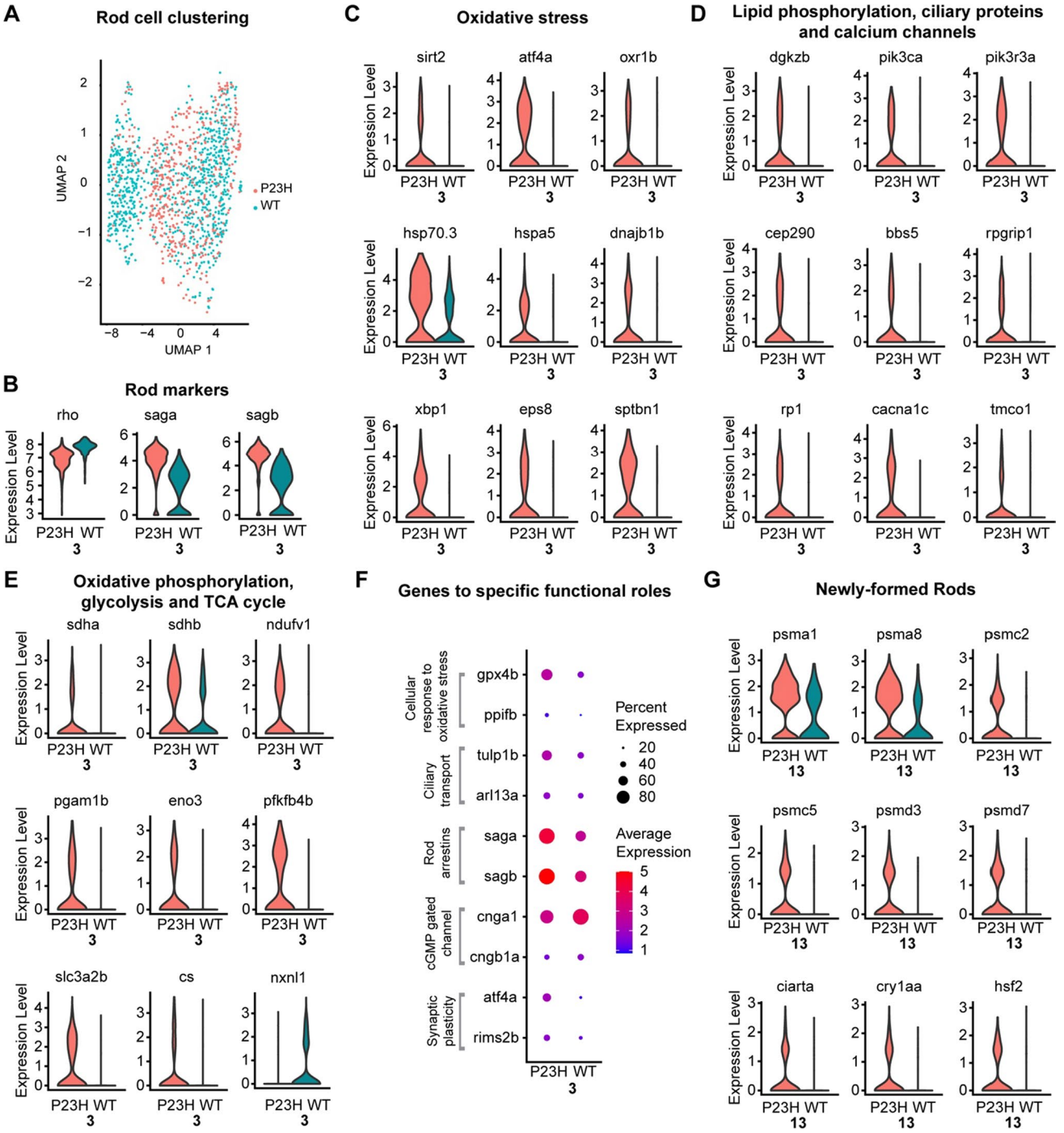

Fig. 3 Transcriptomic analysis of rods and newly formed rods in the WT-P23H integrated dataset reveal an increased response to oxidative stress and misfolded proteins. **A** Overlap of UMAP dimensionality reduction and visualization of rod transcriptomes from WT and P23H transgenic fish. **B** Violin plots showing levels of expression of canonical marker genes in WT and P23H rods. **C**–**E** Violin plots showing expression levels of differentially expressed genes (DEGs) involved in various functional pathways including oxidative stress, response to misfolded proteins, ciliary transport, synaptic remodeling, and metabolism in WT and P23H rods. **F** Dot plot showing the expression level and the percentage of cells expressing DEGs involved in different functional pathways in WT and P23H. **G** Violin plots showing expression levels of DEGs involved in proteasome and ubiquitin-mediated degradation pathway and stress response markers in WT and P23H newly formed rods

proteins (*cep290*, *bbs5*, *rpgrip1*, and *rp1*) and calcium channels (*cacna1c* and *tmco1*) (Fig. 3D).

Metabolism-related differentially expressed genes (DEGs) were upregulated in the P23H rods including oxidative phosphorylation (*sdha*, *sdhb*, and *ndufv1*), glycolysis (*pgam1b*, *eno3*, *pfkfb4b*, and *slc3a2b*) and TCA cycle (*cs* and *ndufv1*) (Fig. 3E). It is possible that the stress due to misfolded protein response leads to increased energy demand that is met by increased oxidative metabolism. Notably, *nxnl1*, the zebrafish homolog of Rod-derived Cone Viability factor, is strongly decreased in P23H rods (Fig. 3E). This factor promotes glucose uptake in cones [32] and potentially rods [33]; its loss could result in reduced glucose uptake forcing a switch from oxidative glycolysis to oxidative phosphorylation to supply cellular energy demand. Our pathway analysis depicts an increase in pathways involved in the synthesis of precursor metabolites, glycolysis, pyruvate metabolism, and TCA cycle to cope with increased stress and energy demand in the P23H rods (Fig S1). It has been shown recently by a multi-omic study that early metabolic imbalance and mitochondrial stress in neonatal photoreceptors lead to cell death in the Pde6b rd1 mouse model of retinal degeneration [34]. Our results correlate with the metabolic changes reported in that study.

Importantly, we noticed an increase in *gpx4b* and *ppifb*, which are involved in the cellular response to oxidative damage, suggesting that rods are experiencing oxidative stress (Fig. 3F). DEGs involved in ciliary transport including *tulp1b* and *arl13a* are also increased in P23H. Mutations in *tulp1* are reported to contribute to ~5% of total RP cases [35] and mutations in *arl13* lead to the failure of rod outer segment formation [36]. Interestingly, we noted a significant increase in the transcript level of rod arrestins (*saga*, *sagb*) in P23H compared to the WT (Fig. 3B, F). The arrestins may be upregulated to compensate for the constitutive activation of P23H mutant rhodopsin, as it has been shown previously that in the mammalian retina stable complexes are formed between mutant rhodopsin and rod arrestin leading to rod cell death [37]. It is implicated that tulp1b is responsible for the ciliary transport of arrestins [38] and the increased arrestins may accumulate in cilia leading to cell death. DEGs involved in cyclic nucleotide-gated channels including *cnga1* and *cngb1a* are both reduced in P23H. Both are involved in the photo-transduction cascade, and their decrease suggests a downregulation of photo-transduction. The DEGs involved in the regulation of synaptic plasticity (*atf4a* and *rims2b*) are upregulated in the P23H, suggesting ongoing remodeling of synapses in P23H rods (Fig. 3F). Previous studies in zebrafish models of rod damage do not reveal such comprehensive transcriptional changes [39–41] and it is important to understand these changes at the molecular level to target therapeutic interventions appropriately.

A newly forming rod cell cluster is evident in P23H

We identified cluster 13 as newly forming rods, as this cluster expresses both progenitor cell markers and rod photoreceptor markers. The progenitor markers including *stmn1a*, *ccnd1*, and *hes*6 are present at a low level, whereas the rod differentiation markers including *fabp7a*, *cxxc5a*, *arl13a*, and *neurod1* are present at high levels in the transcriptome, representing the shift of cells from progenitor state to a differentiated state. This cluster of newly forming rods was not evident in the WT dataset when clustered alone (Fig. 1A), and can be only seen in WT after integrating with P23H for the cluster analysis (Fig. 2A, B). In keeping with the persistent loss and regeneration of rods in the P23H animals, there was a larger number of newly forming rods in P23H (3.8% of cells in the dataset) compared to the WT (1.1% of cells). Functional analysis with ClueGo and Metascape showed that pathways involved in the proteasome and ubiquitin-mediated degradation (UPR), eukaryotic translation, rod cell development, and eye morphogenesis are enhanced in the P23H transcriptome (Fig S1C). The transcripts of genes involved in proteasome and ubiquitin-mediated degradation including *psma1*, *psma8*, *psmc2*, *psmc5*, *psmd3*, *psmd7*, and stress response markers including *ciarta*, *cry1aa* and *hsf2* are more highly expressed in the P23H dataset compared to WT (Fig. 3G), suggesting that even newly forming rods are experiencing stress associated with expression of the P23H mutant rhodopsin.

Cone photoreceptors show markers of stress and changes in metabolic and circadian genes

We initially identified two cone clusters, cluster 2 and cluster 6. The short-wavelength opsin *opn1sw1* is seen in cluster 6 and the long-wavelength opsin *opn1lw1* is enriched in cluster 2 (Fig. 4A). While expression of the P23H mutant rhodopsin is limited to the rods [26], cones in the P23H retina show an increase in the transcriptome of *hsf2*-associated stress response pathway (Fig. 4B), suggesting that cones in this model experience elevated physiological stress. There may be increased oxidative stress in cones due to increased exposure to oxygen in the absence of fully functioning rods, which may lead to increased *hsf2* and subsequent activation of the MAPK signaling pathway [42]. Our data further confirmed the increased expression of *mapk6* in P23H cones compared to WT (Fig. 4B). Cones in the P23H retina also show increased expression of genes for glycolysis and the TCA cycle (*pfkfb3*, *pfkfb4b*, *eno3*, *cs*, *aco2*, and *got1*) (Fig. 4B), but like rods, expression of *nxnl1* is reduced in cones. These results imply that cones rely on aerobic metabolism, but that glucose supply could be limiting. It has been shown previously that aerobic glycolysis in

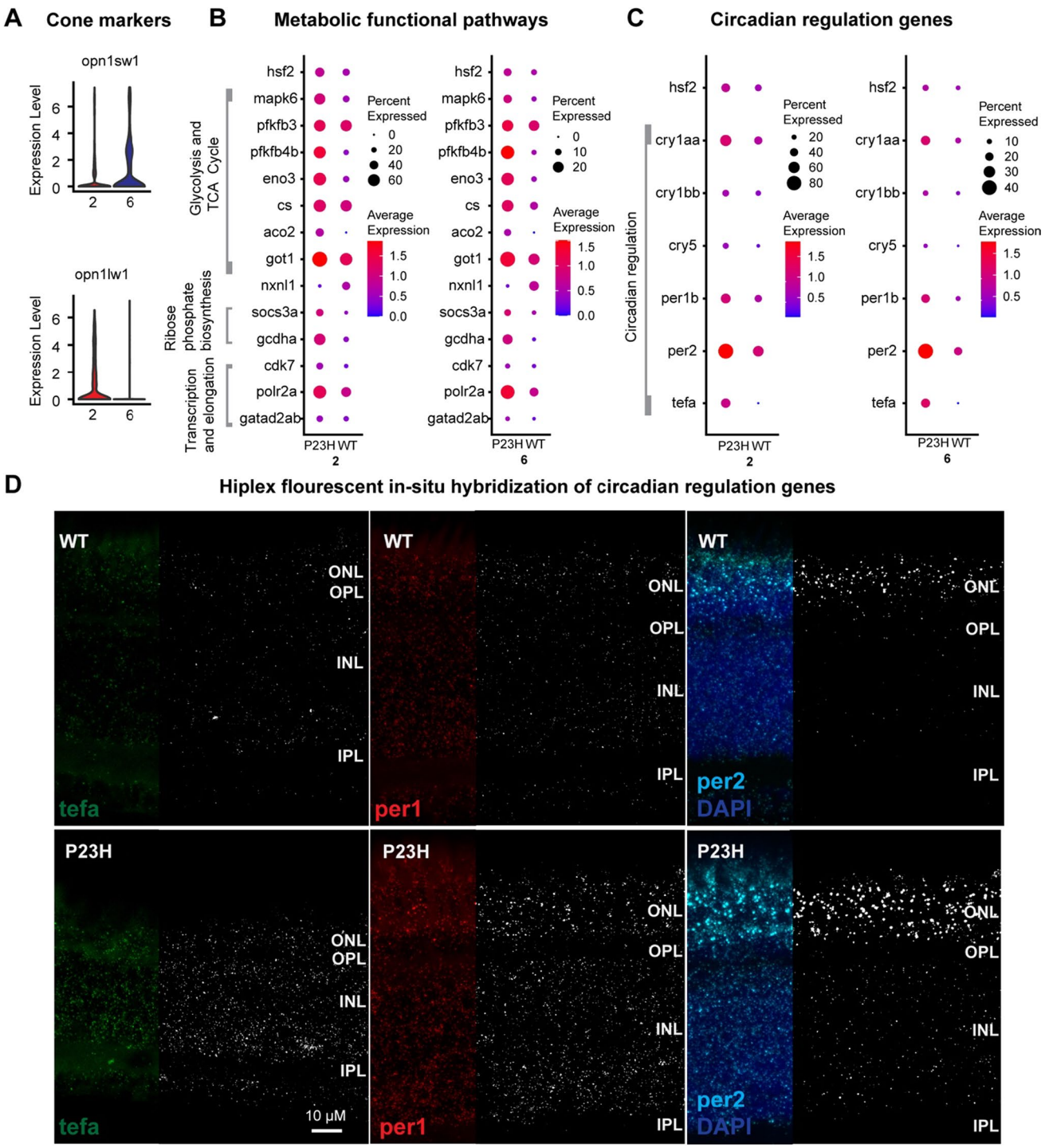

Fig. 4 Comparative transcriptomic analysis of cones in WT-P23H integrated dataset reveals changes in metabolism and circadian regulation. **A** Violin plots showing levels of expression of short- and long-wavelength opsins in cone clusters 2 and 6. **B** Dot plot showing the expression level and the percentage of cells expressing DEGs involved in different metabolic functional pathways between WT and P23H. **C** Dot plot showing the expression level and the percentage of cells expressing DEGs involved in circadian regulation between WT and P23H. **D** Hiplex fluorescent in situ hybridization for *tefa*, *per1*, and *per2* in sections of adult retina. The fluorescent product is shown in the left third of each image, while the remainder displays a binary mask in the fluorescent in situ hybridization product channel. All three genes show increased expression throughout the retina in P23H compared to WT, reflecting the changes captured by single-cell transcriptome analysis. Scale bar applies to all panels

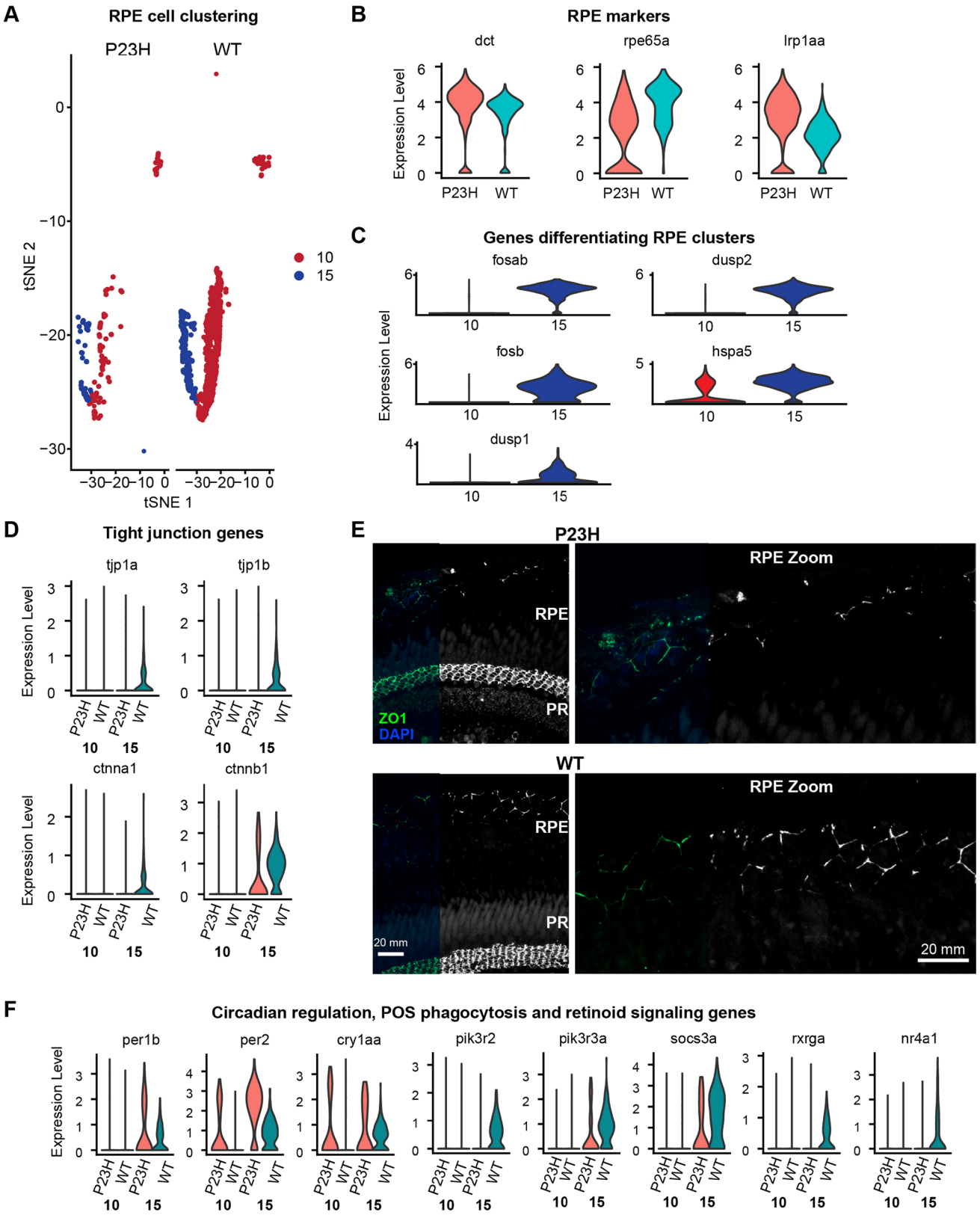

photoreceptors is essential for normal rod function and is a metabolic choice that augments cone function and survival during nutrient-stress conditions [43]. We also noticed increased expression in DEGs involved in ribose phosphate biosynthesis (*socs3s* and *gcdha*) and RNA polymerase II transcription and elongation (*cdk7*, *polr2a*,

◂**Fig. 5** RPE transcriptome is altered in the RP model. **A** tSNE map showing the proportions of RPE cells found in the P23H and WT retinal samples. **B** Violin plots showing levels of expression of canonical RPE marker genes in WT and P23H RPE cells. **C** Violin plots showing expression levels of DEGs differentiating RPE clusters 10 and 15. **D** Violin plots showing expression levels of genes involved in tight junctions in WT and P23H RPE. **E** Immuno-fluorescent labeling of tight junction protein ZO1 in retina of adult P23H and WT zebrafish. The layer of retinal pigmented epithelium (RPE) is at the top. Additional strong ZO1 labeling below the photoreceptor inner segments (PR) is the outer limiting membrane formed by Müller cell end-feet tight junctions. Right panels show magnified view of ZO1 labeling in the RPE. Scale bars in WT apply to both WT and P23H. **F** Violin plots showing levels of expression of DEGs including those involved in circadian regulation, POS phagocytosis and retinoid signaling in WT and P23H RPE cells

and *gatad2ab*) (Fig. 4B). Sufficient supplies of NADPH, ATP, and the metabolic intermediates ensure rapid macromolecular synthesis underlying the continuous self-renewal of cone OS and the demand may be increased to cope with the increased stress.

The *hsf2*-associated stress response pathway includes increased levels of *cry1a* and *nr1d2b*, which are shown to be involved in circadian function [44]. It has been shown that in zebrafish larvae, the expression of *hsf2* was concomitant with the expression of genes involved in the response to oxidative stress and chaperone genes, and it occurs in phase with *cry1a* and other genes that belong to the negative arm of the transcriptional regulation network of the circadian rhythm [45]. We examined the transcriptome profile of other molecular circadian regulators and found that the circadian regulators *cry1aa*, *cry1bb, per1b*, *per2*, and *tefa* were increased in the P23H cones compared to the WT (Fig. 4C). To validate the single-cell transcriptome data, we examined the expression of *per1*, *per2*, and *tefa* using multiplex in situ hybridization. The results demonstrate the increased expression of *per1*, *per2*, and *tefa* in the P23H retina compared to the WT (Fig. 4D). Increased levels of expression of all three genes were detected in both the outer nuclear layer (ONL), harboring photoreceptors, and in the inner nuclear layer (INL), occupied by numerous other cell types. The overall increased expression of these circadian cycle genes in P23H tissue samples compared to WT tissue samples is consistent with our single-cell data. Disruption of behavioral and retinal circadian rhythms has recently been reported in a mouse model of RP due to an RNA splicing factor mutation [46], suggesting commonality in pathology. Overall, these changes suggest that the cones undergo comprehensive modifications including metabolism and circadian activity during the degeneration/regeneration scenario.

RPE tight junction genes and stress-protective mechanisms are lowered in the RP model

The zebrafish retinal transcriptome showed two different RPE clusters, clusters 10 and 15 (Fig. 5A). Both RPE cell clusters express the canonical RPE genes *rpe65a*, *dct* and *lrp1aa* (Fig. 5B) but are segregated due to the presence of transcriptome that enriches for different functional pathways (Fig S2). Differential expression analysis revealed that cluster 15 has many unique transcripts that were not expressed in cluster 10 (Fig. 5C). The 5 most up-regulated genes in RPE cluster 10 were RNA-binding proteins including *rpl3*, *rpl4*, *rpl5a*, and *rpl6*, which enable protein translation; these were also present in cluster 15. Functional pathways involved in phagocytosis, endocytosis, lysosome, oxidative stress and drug metabolic process are all enriched in cluster 15, whereas cluster 10 showed pathways involved in translation and ribosome assembly (Fig S2). The receptor tyrosine kinase *mertka* involved in RPE phagocytosis of photoreceptor outer segments (POS) [47] is highly expressed in cluster 15, suggesting active phagocytosis in these RPE cells. RPE cells have been categorized into multiple subpopulations based on their location and morphology [48–51]. While our data do not have the spatial resolution to differentiate RPE subpopulations by location and morphology, the 2 subpopulations of RPE cells in our data are functionally consistent with subpopulations found in previous studies based on transcriptomic functional activities [52, 53].

We have seen a drastic decrease in the number of RPE cells in the P23H RP model compared to the WT (Fig. 5A, E), which is consistent with several previously reported studies that when the rods are lost oxygen continues to flow into the outer retina from the choriocapillaris, creating a hyperoxic environment that is presumably hostile for the remaining cells [54, 55]. In some retinal degeneration models, disruption of RPE tight junctions is observed, affecting the integrity of RPE cells [17, 56]. Analysis of the DEGs in RPE cells involved in tight junction formation, including *tjp1a*, *tjp1b*, *ctnna1*, and *ctnnb1*, revealed a decrease in the P23H compared to the WT (Fig. 5D). Immunostaining for tight junction protein ZO-1 confirmed that tight junctions in the P23H RPE were disrupted when compared to WT (Fig. 5E). In some areas of the P23H retina, the tight junctions were almost completely absent (Fig. 5E). This suggests that RPE tight junction disruption is a pathological effect in RP that is conserved across species. We also note that the tight junction pathology and reduced photoreceptor outer segment lengths may have influenced the number of RPE cells captured during preparation of the single-cell libraries, potentially contributing to the reduced number of RPE cells found in P23H fish.

Ongoing degeneration and regeneration in the P23H RP model had a significant impact on several other aspects of the RPE transcriptome. We have noticed an increase in circadian genes, such as *per2*, *per1b*, and *cry1aa*, in the P23H dataset (Fig. 5F), similar to that seen in cones, suggesting the change is coordinated between RPE and photoreceptors. It has been shown in previous studies that *per2* regulates POS phagocytosis in RPE cells [57], suggesting a change in the rhythm of POS phagocytosis in the RP model. The phosphoinositide 3-kinase regulators *pik3r2, pik3r3a*, and *socs3a* are reduced in the P23H retina compared to the WT (Fig. 5F). It has been shown in previous studies that the activation of the PI3K-Akt pathway protects RPE cells against the deleterious effects of oxidative stress that occur due to POS phagocytosis [58, 59]. These protective mechanisms seem to be reduced in the RPE of P23H zebrafish.

The retinoid X receptor *rxrga* and nuclear receptors *nr4a1* and *nr4a3* are lowered in the P23H dataset compared to the WT (Fig. 5F). NR4A receptors heterodimerize with RXR receptors and activate transcription in a 9-cis retinoic acid-dependent manner. They can also repress inflammatory gene promoters by recruiting corepressor complexes [60]. This complex suite of transcriptome changes suggests that the RPE cells lose several stress-protective mechanisms during the degeneration–regeneration scenario.

Rod bipolar cells show evidence of stress and neuronal remodeling

We have identified three different bipolar cell clusters, 0, 20 and 23 in our dataset; each cluster expressed a specific set of markers (Fig. 6A). The rod bipolar cell marker *prkca* [22] is highly enriched in cluster 20 (avg. expression 2.7) and to a minor extent in cluster 0 (avg. expression 0.7) only in very few cells (Fig. 6B). Because of the high expression of *prkca*, we considered cluster 20 likely to be the rod-dominated mixed bipolar cell [61] that forms most synaptic contacts with rods. All of the bipolar cell clusters displayed differences in transcriptome profile between the WT and P23H (Fig. 6B), including downregulation of neuronal specification genes *neurod4* and *nrxn3b* and upregulation of stress-related genes including *ubl3a*. A prominent change in all bipolar cell clusters is the dramatic upregulation of *rgs16* (Fig. 6B), which accelerates the offset of G protein signaling [62, 63], potentially modifying signaling by metabotropic glutamate receptors, dopamine receptors, or other GPCRs.

We focused on cluster 20 to examine the influence of rod degeneration and regeneration on gene expression. Genes involved in synaptic vesicle trafficking including *snap25a, snap25b* and *nsfa* are increased in the P23H dataset compared to the WT (Fig. 6C). This suggests that there may be compensation at the bipolar cell output synapses for the reduced rod input in P23H retina. We also detected increases in the transcriptome of some genes involved in the stress response including *dnajb1b*, *hspd1*, *sod1*, and *gsto1* in the P23H dataset compared to the WT (Fig. 6C). As we found in cones and RPE, levels of *per1b*, *per2*, and *tefa*, which are involved in circadian regulation, were elevated (Fig. 6C). This suggests that rod photoreceptor loss leads to circadian changes that are reflected throughout the retina, consistent with the increased expression detected throughout the retina in the in situ hybridization experiments (Fig. 4D).

The overall comparison between WT rod bipolar (RBP) transcriptome and P23H RBP transcriptome with STRING, which infers protein–protein interaction networks, suggests that the interaction network changes in the P23H RBP cells when compared to WT. P23H RBP display far fewer annotated interactions, and the top enriched pathways are different between WT and P23H (Table S5). Pathways for ATP synthesis and reactive oxygen species (ROS), and reactive nitrogen species (RNS) production were enriched in the P23H RBP transcriptome, suggesting increased energy demand and stress response in the P23H RBP cells (Table S5). Thus, physiological remodeling in the P23H RBP cells involves a complex interplay of oxidative stress, synaptic remodeling and synaptic transmission.

Horizontal and amacrine cells show changes in genes regulating axonal remodeling in the P23H RP model

We identified the horizontal cells using the markers *rprmb, aqp9a* and *mdka* (Fig. 7A). The gap junction proteins *cx52.6, cx52.9, and cx55.5* are all uniquely enriched in the horizontal cells, serving as additional marker genes (Fig. 7B), and showed no significant differences between WT and P23H retinas. We studied the differences between the horizontal cells in WT and P23H by functional analysis (Fig S3) and identified increased expression of genes involved in axon remodeling and microtubule stability including *apc2, camsap1b, sptbn1, sqstm1*, *ndel1a*, and zgc*:92,606* (Fig. 7A). Previous studies have shown that *apc2* and *camsap1* play an essential role in axonal projections through the regulation of microtubule stability [64, 65]. Structural remodeling of horizontal cells, including neurite sprouting, is a well-documented phenomenon in models of retinal degeneration [66], in keeping with these findings. Functional annotation of genes differentially expressed in WT and P23H horizontal cells show response to nitrogen starvation GO enriched in P23H suggesting an increase in autophagy and organelle disassembly (Fig S3), indicating ongoing cellular stress.

We have identified six clusters of amacrine cell types with our initial clustering analysis including clusters 1, 5, 11, 19, 21, and 22 (Fig. 2B). Cluster 1 was identified as GABAergic amacrine cells due to the specific enrichment

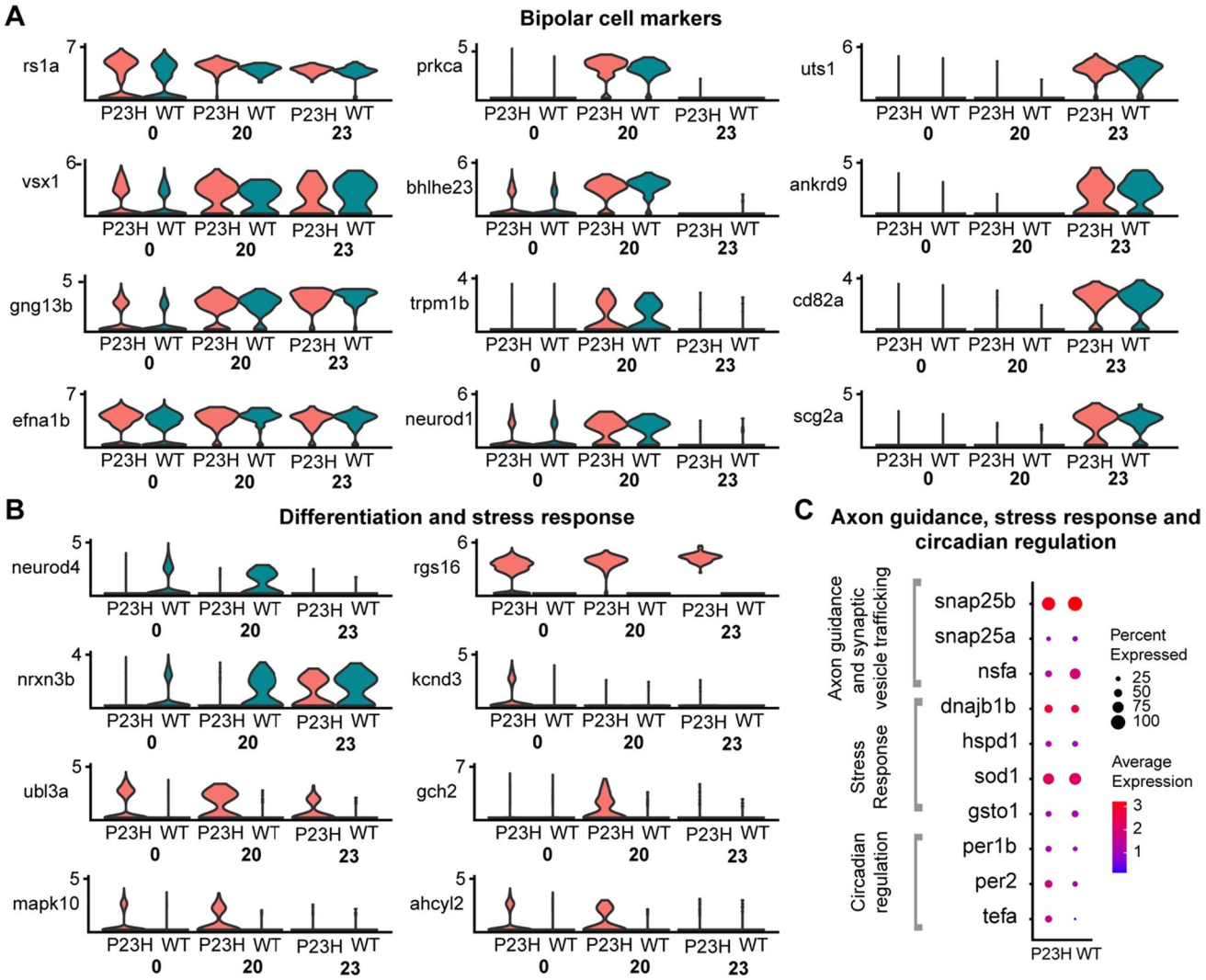

Fig. 6 Comparative transcriptomic analysis of bipolar cell clusters in the WT-P23H integrated dataset shows evidence of stress and neuronal remodeling in the RP model. **A** Violin plots showing levels of expression of specific marker genes in different clusters of bipolar cells (0, 20, and 23). **B** Violin plots showing changes in expression of genes involved in differentiation and stress response in the three bipolar cell clusters. **C** Dot plot showing the expression level and the percentage of cells expressing DEGs involved in axon guidance, stress response and circadian regulation between WT and P23H in cluster 20

of the *gad2*, which is involved in GABA neurotransmitter biosynthesis (Fig. 7C). The glycinergic amacrine cells were identified by the enrichment of glycine transmembrane transporter *slc6a9* in cluster 5. Cluster 11 was identified as starburst amacrine cells due to the enrichment of both *gad2* and *chata*. Cluster 19 contained the unique enrichment of *calb1* and *calb2a* without the presence of glycine or GABA transporters (Fig. 7C). In the past, studies have reported this kind of unique amacrine subpopulation [67] and it is interesting to see these data captured at a single-cell level even without enrichment of amacrine cells. This amacrine subset also shows the high expression of *nxph2a*, which is a signaling molecule that resembles neuropeptides [68]. Clusters 21 and 22 both express cholinergic markers *chata*, *slc18a3a* along with *chgb*, and are differentiated in that cluster 22 is GABAergic (expressing *gad2*) while cluster 21 is glycinergic (expressing *slc6a9*; Fig. 7C). Both of these clusters also share high similarities with the retinal ganglion cell (RGC) transcriptome. All six amacrine cell clusters are present in both WT and P23H.

Changes in gene expression in amacrine cells were relatively modest between WT and P23H retina. We see the increased expression of *glula* in amacrine cell clusters in P23H (Fig. 7D). Further, the ionotropic glutamate receptors *gria2a, gria3a, grin1b, and grin2aa* are all increased in P23H amacrine cell clusters compared to WT, suggesting the possibility of increased excitatory current (Fig. 7D). We noticed small increases in genes that

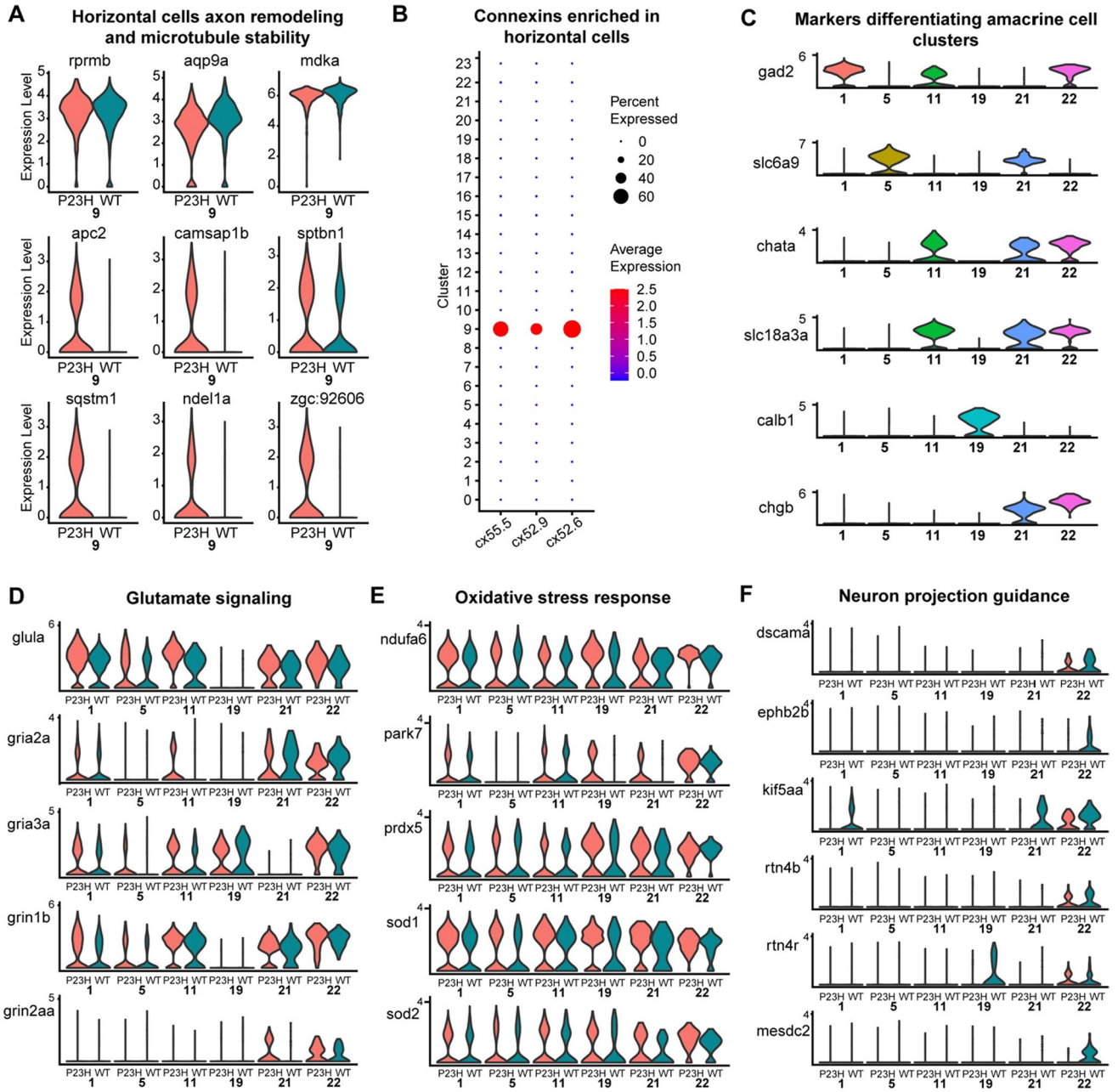

Fig. 7 Transcriptomic analysis of Horizontal and Amacrine cells in the WT-P23H integrated dataset reveals changes in axon remodeling in the RP model. **A**, **B** Horizontal cells; **C**–**F** Amacrine cells. **A** Violin plots showing levels of expression of canonical marker genes as well as DEGs involved in axon remodeling and microtubule stability in WT and P23H horizontal cells. **B** Dot plot showing the specific enrichment of *cx52.6*, *cx52.9,* and *cx55.5* in horizontal cell cluster (9) compared to all other retinal cell types. **C** Our data identified six different types of amacrine clusters (1, 5, 11, 19, 21, and 22). Violin plots showing levels of expression of canonical marker genes expressed in different amacrine clusters. **D**–**F** Violin plots showing levels of expression of DEGs involved in glutamate signaling (**D**), oxidative stress response (**E**), and neuron projection guidance (**F**) between WT and P23H amacrine cells

respond to oxidative stress and ROS, including *ndufa6, park7, prdx5, sod1* and *sod2* (Fig. 7E). We also detected a reduction in the expression of a few genes involved in neuron projection guidance [69] including *dscama, ephb2b, kif5aa, rtn4b*, *rtn4r,* and *mesdc2* (Fig. 7F), suggesting some loss of neuronal wiring specificity in P23H amacrine cells.

Retinal ganglion cells show disturbances in the normal synaptic activity in P23H transgenic fish

Retinal ganglion cells in animal models of RP are characterized by aberrant spontaneous activity [18, 20]. We identified the RGCs through the enriched presence of the markers *pou4f1, rbpms2a* and *rbpms2b*, identifying cluster 8 (Fig. 8A). In keeping with increased spontaneous activity observed in other RP models, pathway analysis of RGCs showed that certain genes involved in the regulation of synaptic transmission, especially glutamatergic synapses including *grin2aa, shank2*, and *cacng2a*, are enriched in the P23H dataset compared to the WT (Fig. 8B). Further analysis revealed the increase of glutamate receptors including *grin1b*, *grin2aa*, *gria2a*, *gria2b* and *gria3a* as well in the P23H retina, suggesting changes in sensitivity to glutamatergic input due to photoreceptor degeneration (Fig. 8C). These are differentially expressed genes associated with glioma in previous studies [70]. Transcripts of genes involved in active transport and ATP synthesis including *atp1b1b* and *atp1a3a, atp5a1, atp5l*, and *atp2a2b* are increased in the P23H dataset (Fig. 8B). We noticed increased expression of transcripts involved in succinate dehydrogenase complex and electron transport chain including *sdha*, *sdhb*, *sucla2*, and *suclg1*, suggesting the remodeling due to photoreceptor degeneration leads to enhanced oxidative metabolism, possibly in response to increased energy demand (Fig. 8B). Heat shock protein *hspd1* (HSP60) is highly enriched in the P23H RGCs compared to the WT (Fig. 8D) and may reflect the role of this protein as a cellular defense mechanism in response to stress. The increases in expression of genes supporting responses to glutamatergic input and increased spontaneous activity observed in other RP models suggest that RGCs are at risk for glutamate excitotoxicity. It has been shown in a previous study that the HSP60 levels are high in the RGCs of glaucomatous eyes compared to normal eyes [71]. Finally, we also noticed an increase in Wnt signaling components in the P23H retina compared to the WT including *kras*, *foxo3a*, *rac3b* and *dctn2* (Fig. 8D). It has been shown in previous studies that Wnt signaling regulates several aspects of RGC biology, including differentiation, proliferation and axonal outgrowth [72], and may reflect an increase in synaptic remodeling in the P23H retina.

Phagocytic and apoptotic regulators are increased in P23H microglia/macrophages

We identified two microglia/macrophage clusters in the integrated zebrafish retina dataset, clusters 16 and 17, using the markers *cd74*a, *cd74bB* and *pfn1* (Fig. 9A). Cluster 16 showed the enriched presence of many markers including *apoc1*, *ccl34b.1* and *fabp11a*, whereas cluster 17 had the enriched presence of *ccl36.1*, *trac*, and *zap70* (Fig. 9B). A recent study has reported the presence of two phenotypically and functionally distinct microglial populations in adult zebrafish, segregated by the presence of *ccl34b.1* [73]. We differentiate the microglial clusters based on the presence

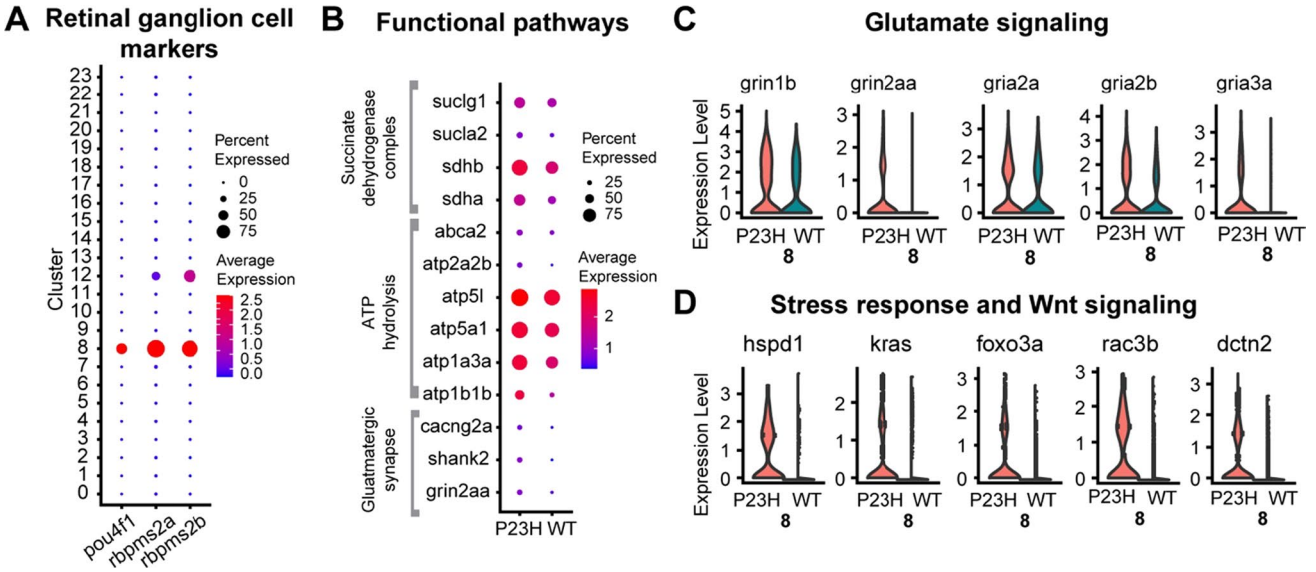

Fig. 8 Comparative transcriptomic analysis of retinal ganglion cells in WT-P23H integrated dataset. **A** Dot plot showing the specific enrichment of canonical markers *pou4f1*, *rbpms2a* and *rbpms2b* in the RGC cluster compared to all other retinal cell types. *rbpms2a* and *rbpms2b* are present at lower levels in Müller glial cells (12) as well. **B** Dot plot showing the expression level and the percentage of cells expressing DEGs involved in different functional pathways between WT and P23H. **C**, **D** Violin plots showing increased levels of expression of DEGs involved in glutamate signaling (**C**), stress response and Wnt signaling (**D**) between WT and P23H RGCs

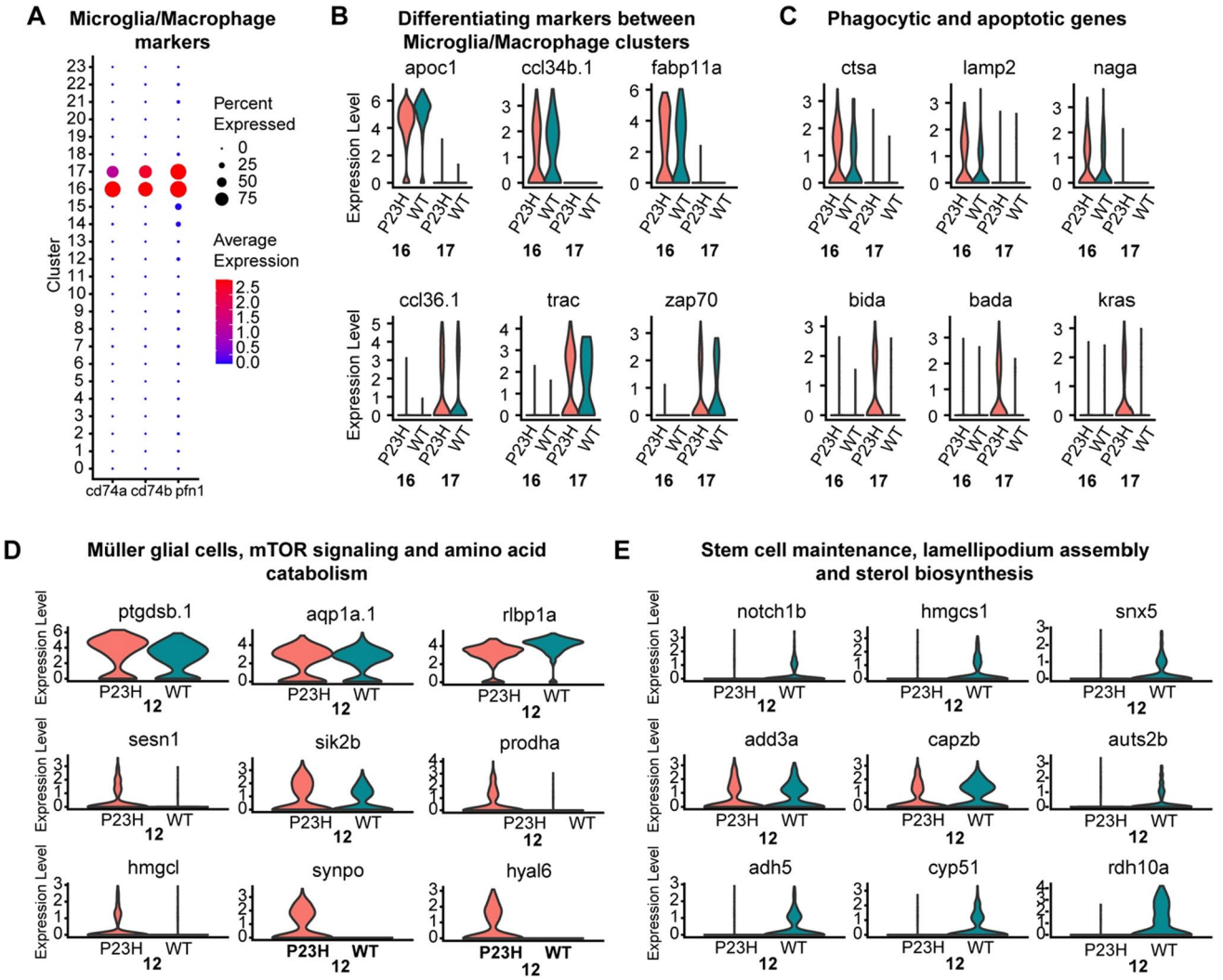

Fig. 9 Comparative transcriptomic analysis of microglial/macrophage clusters and Müller glial cells in the zebrafish retina**. A–C** Microglia/Macrophages; **D**, **E** Müller glial cells. **A** Dot plot showing the specific enrichment of canonical markers *cd74a* and *cd74b*, as well as the non-canonical marker *pfn1* in the microglia/macrophage cell clusters. **B** Violin plots showing the expression of cluster-specific markers between the two microglial/macrophage clusters (16 and 17). **C** Violin plot showing the expression of increased phagocytic and apoptotic markers in P23H microglia/macrophages. **D** Violin plots showing the specific enrichment of canonical Müller glial cell markers as well as changes in DEGs involved in mTOR signaling and amino acid catabolism. **E** Violin plots showing the decreased levels of DEGs involved in stem cell maintenance, lamellipodium assembly and sterol biosynthesis in P23H Müller glia

of *apoc1* and *apoc1* positive cluster 16 also shows the specific presence of *ccl34b.1* in our study. Another interesting study in the zebrafish retina has identified the regeneration-associated transcriptional signature of retinal microglia and macrophages using RNA seq [74] and most of the top 50 markers discussed in that study are captured in our single-cell analysis along with the specific type of microglia.

In the P23H fish, certain phagocytic markers like *ctsa*, *lamp2*, and *naga* are increased in cluster 16, whereas we see the increase of *bida*, *bada*, and *kras* involved in the positive regulation of apoptosis in cluster 17 (Fig. 9C). Functional analysis revealed differences between two microglial clusters: cluster 16 enriched with *apoc1* shows increased phagocytic and lytic activity along with cell chemotaxis and translation elongation, whereas cluster 17 shows the annotation for apoptosis, myeloid cell homeostasis and regulation of the immune system (Fig S4). Many studies have shown that an immune response is necessary for the regeneration process [75, 76]. We believe that cluster 16 plays an important role of clearing out cells throughout degeneration while cluster 17 may play a role necessary for regeneration. Our data also provide several new molecular markers associated with microglia.

Müller glia show increased proliferative function in the P23H RP model

Müller glia are the center of attention in studies examining the regeneration of neurons in the retina. Following retinal injury, zebrafish Müller glia can reprogram to become multipotent progenitor cells with the ability to differentiate into many types of neuron [25, 77]. We identified the Müller glia cluster 12 with the highly enriched expression of markers *ptgdsb.1*, *ptgdsb.2, aqp1a.1*, and *rlbp1a* (Fig. 9D). Several transcriptional changes suggest that the Müller glial cells in the P23H chronic degeneration/regeneration model are tending toward their proliferative role and downregulating genes involved in the normal maintenance functions. Functional analysis showed enhanced TOR signaling and chromatin assembly or disassembly pathways in P23H whereas sterol biosynthesis and regulation of lamellipodium assembly were downregulated relative to the WT (Fig S5). Further analysis of the transcriptome showed the increased expression of mTOR pathway regulators *sesn1* and *sik2b* in the P23H dataset (Fig. 9D); *synpo*, an actin-associated protein that modulates dendritic spine shape, is also enriched in the P23H Müller glial cells. We also noted an increase in *hmgcl* and *prodha* involved in the amino acid catabolic process in the P23H (Fig. 9D). Interestingly we also see a uniquely enriched expression of *hyal6* (hyaluronoglucosaminidase 6) in the P23H Müller glial transcriptome (Fig. 9D). It has been shown previously in zebrafish studies that shorter forms of hyaluronic acid contribute to the regenerative process in both larval and adult zebrafish [78, 79]. In the meantime, we see the unique reduction of markers for stem cell population maintenance including *notch1b*, *hmgcs1* and *snx5* in the P23H dataset compared to WT (Fig. 9E). We likewise see the decreased expression of genes involved in lamellipodium assembly, such as *add3a, capzb*, and *auts2b*, as well as in sterol biosynthesis, including *adh5*, *cyp51*, and *rdh10a* (Fig. 9E) in the P23H Müller glial transcriptome. Thus, Müller glia in the chronic retinal degeneration/regeneration model have shifted their transcriptional landscape to be poised to support proliferation.

Retinal progenitor cells (RPCs) especially the rod progenitors are enriched in the P23H RP zebrafish

The RPC population (cluster 14) was identified by the expression of proliferative stem cell markers including *ccna2, ccnb2, ccne2*, and *stmn1a* (Fig. 10A). The P23H dataset contains a highly enriched amount of transcripts specific for mitotic cell division including *aurkb*, *top2a*, and *ube2c*, suggesting a highly proliferative cell cluster in the P23H, whereas the WT transcriptome shows the enrichment of markers for pluripotent retinal progenitor cells including *foxn4*, *crabp2a*, *notch1b* and *her15.1* (Fig. 10A). It is very important to note that we identified a cluster of RPCs even in the WT, suggesting that neurogenesis in zebrafish is a very common phenomenon carried out to maintain the dynamic balance in the growth of eye size related to its body size. This also shows the power of single-cell profiling, which can identify small populations of cells in the tissue that might not be noticed in other types of analysis. The RPC population in WT is much smaller (~62 cells) compared to the P23H (~341 cells). Functional pathway analysis shows the enrichment of Notch signaling, FoxO signaling pathway, and TGF-B signaling pathway in the WT RPCs, whereas mitotic cell cycle and proteasome pathway, DNA replication, and chromosome organization are all enriched in P23H RPCs (Fig. 10B). These analyses further support the interpretation that RPCs in the P23H retina maintain a more higly proliferative state than in the WT, in keeping with the ongoing photoreceptor regeneration in this model.

Neurogenic progenitor cells are identified in both WT and P23H zebrafish retina

We identified a separate group of neurogenic progenitor cells (NPCs), cluster 7, which resemble committed neuronal cells but show the presence of several progenitor markers including *marcksl1a*, *marcksl1b*, *atoh7*, and *myca*. It has been reported recently that two transcriptionally distinct progenitor clusters including the proliferative and neurogenic progenitors are seen in developing zebrafish retina [25]. Our data confirm that these clusters are seen also in the zebrafish adult retina supporting the continuous growth of the zebrafish eye. This cluster differed transcriptionally between WT and P23H. Transcripts of certain genes involved in the cAMP response, including *junba*, *junbb* and *rgs16*, showed increased expression in P23H whereas transcripts involved in the regulation of cytoskeleton structure including *tubb5*, *tuba1c* and *tuba8l4* are reduced (Fig. 10C). The group of chaperonin T-complex protein genes involved in neuronal development and eye morphogenesis [80], including *cct2*, *cct3*, *cct4*, *cct5*, and *cct7* is decreased in the P23H NPCs compared to the WT (Fig. 10D). The P23H NPCs also express a reduced amount of certain immunoproteasome subunits including *psma1*, *psmb1*, *psmb2*, *psmb3*, *psmb6*, and *psmb7* (Fig. 10D). It has been shown that proteasomes are essential in maintaining the self-renewal of neural progenitors and the proteasomes decrease with aging [81]. The P23H degeneration condition may mimic aging due to chronic stress and hence we notice a decrease in the chaperone and proteasome DEGs.

Overall, this study provides a comprehensive transcriptome analysis of most of the predominant retinal cell types of the zebrafish retina and a first-time comprehensive analysis of the transcriptome changes happening in every

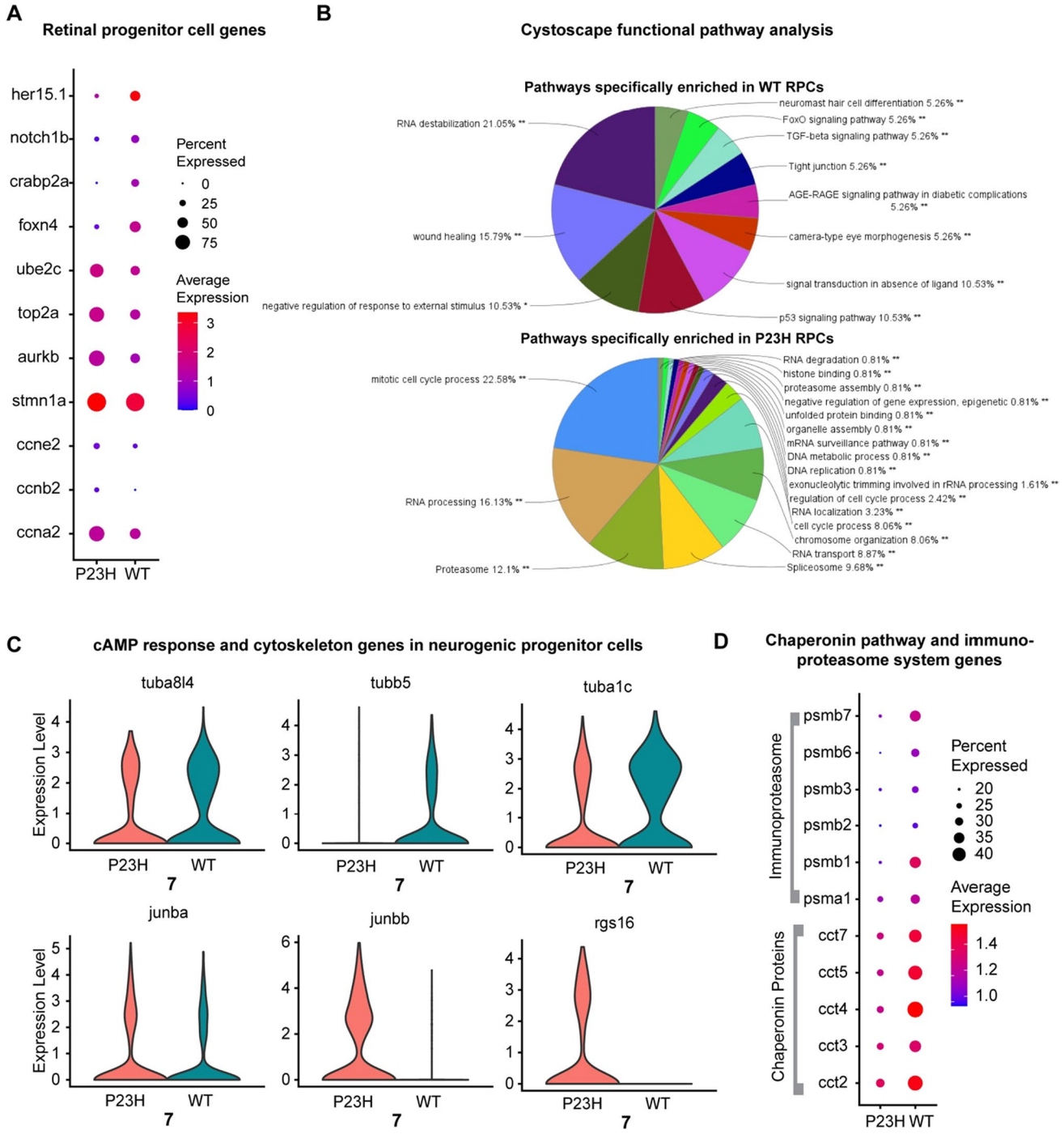

Fig. 10 Retinal progenitor cells (RPCs) are enriched in the RP model whereas a neurogenic progenitor cell (NPCs) cluster was identified in both WT and P23H**. A**, **B** RPCs; **C**, **D** NPCs. **A** Dot plot showing the expression level and the percentage of cells expressing WT (*her 15.1*, *notch1b*, *crabp2a*, *foxn4*) and P23H specific (*ube2c*, *top2a*, *aurkb*) RPC markers. **B** Cytoscape functional pathway analysis pie charts showing the functional pathways that are specifically enriched in WT vs. P23H RPCs. **C** Violin plots showing changes in DEGs involved in cAMP response and cytoskeleton structure between WT and P23H NPCs. **D** Dot plot showing the changes in expression level and percentage of cells expressing DEGs involved in the chaperonin pathway and immunoproteasome system in WT and P23H NPCs

retinal cell type during RP in a regeneration-enabled zebrafish model.

Discussion

The development of precise molecular and cellular strategies for regeneration- or transplantation-based therapies for RP requires a comprehensive understanding of how the entire retinal landscape is affected. Cell type-specific changes and cellular heterogeneity that comprise retinal remodeling during RP play important roles in the integration of new cells and effective signal transmission. Interventions that presume substantial preservation of the neural retina will likely fail in the late stages of the disease.

In mammalian studies, retinal remodeling has been studied extensively through different animal models, modes of degeneration, and time points after onset of damage. Collectively, it has been found that retinal remodeling in the context of rod degeneration occurs through 5 phases [82, 83]. In phase 0, the retina is healthy and there is no loss of photoreceptors [83]. As the initial stress and degeneration of photoreceptors begins, retina remodeling has entered phase 1 [82, 83]. In this phase, rod bipolar cells and rod-contacting horizontal cells retract their dendrites from rod spherules and assume immature synaptic structures, with a subset of them making contacts with cone pedicles [12, 83–85]. As cone photoreceptors are progressively lost via the bystander effect, retinal remodeling enters phase 2 [82, 83]. Cone photoreceptors begin to lose their outer segments and synaptic pedicles and eventually degenerate [86]. During this phase, Müller glial cells (MGCs) become hypertrophic and reactive [82, 83, 87]. Both bipolar cells and horizontal cells sprout new neurites; neurites from horizontal cells extend into the INL [82, 83, 88, 89]. Rod bipolar cells reprogram to shift expression of their receptor phenotypes and become pharmacologically consistent with OFF bipolar cells [83]. Dendrites of cone bipolar cells lose continuity and complexity as more cones degenerate [12, 82, 89, 90]. Retinal remodeling enters phase 3 only after complete loss of cone photoreceptors [82, 83]. During this phase, there is widespread neurite sprouting in bipolar cells, horizontal cells, amacrine cells and retinal ganglion cells [82, 83]. Deafferentation is seen throughout the retina. Eventually, retinal remodeling enters phase 4, where proteinopathies progressively degenerate the remaining neurons in the retina [83].

Our single-cell transcriptome analysis identified molecular pathways that are dysregulated in each retinal cell type in an RP model with ongoing regeneration, allowing us to create an extensive atlas of cellular changes. While rod degeneration is severe in this model [26], ongoing regeneration maintains the retina in the equivalent of phases 1 and 2 in mammalian models with retinal degenerative diseases (RD). In a previous study, we showed that cone photoreceptors did not degenerate, but did have shorter outer segment lengths that are consistent with characteristics of phase 2 of retinal remodeling [26]. We found that chronic degeneration and regeneration of rods affects all retinal cell types. Transcriptional changes were diverse, reflecting widespread oxidative stress, modifications of metabolism, and changes in circadian rhythm, glutamate signaling and synapse remodeling.

Rod photoreceptor degeneration reduces oxygen consumption in the outer retina and leads to increased oxygen tension that can have damaging consequences for other cells in the outer retina [91]. A disparity between ROS production and antioxidant capacity leads to oxidative damage, which has been reported in many previous studies [5, 55]. Both mature rods and newly forming rods in the P23H retina display increased levels of oxidative stress markers. Our data indicate that while rods are undergoing oxidative stress, the rest of the retina mounts an extensive response against its progression. Furthermore, proximity to the degenerating rods plays a role in the level of response observed. In cones, RPE and bipolar cells, antioxidant genes, such as *sod1*, *sod2,* and *hsf2*, are highly upregulated to help minimize oxidative damage. Retinal neurons further away from rods, such as amacrine cells, are still responding to oxidative stress, but to a lesser extent.

The retina is one of the most energy-demanding tissues in the body, with very high demand driven by photoreceptors. Despite rod photoreceptor loss in the P23H retina, we see a host of metabolic changes throughout the retina that suggest adaptations to increased energy demand. Glycolysis and TCA cycle enzymes are increased in both rods and cones. While in rods this could be due to increased energy demand to deal with misfolded protein, the notable downregulation of Rod-derived Cone Viability Factor *nxnl1* in rods and cones suggests that glucose uptake could be compromised [32], leading to nutrient starvation and potentially compensatory upregulation of glycolytic and TCA cycle genes. In the inner retina, retinal ganglion cells displayed increased expression of mitochondrial electron transport chain genes, which may reflect energy demand derived from elevated spontaneous activity.

Previous studies have shown that ROS activate glycolysis [92], which may provide a parallel mechanism to upregulate glycolysis in the outer retina. Glycolysis intermediates are substrates for glycan synthesis, the pentose phosphate pathway (PPP), and serine synthesis pathway. All of these pathways are upregulated in the P23H retina compared to the WT retina. Such a shift in metabolism has been found to be essential in both tail regeneration and cardiomyocyte proliferation and regeneration after injury in adult zebrafish [93, 94]. Combined with our results, these observations suggest that a metabolic shift toward glycolysis is pronounced during regeneration and needs to be considered for retinal regeneration therapy.

Our data show evidence for significant synapse and axon remodeling throughout the retina in the P23H zebrafish. In the rods and cones, genes involved in the regulation of neurotransmitter levels, neurotransmitter release, and regulation of synaptic plasticity are upregulated in the P23H retina, while genes involved in axon guidance and axon extension are reduced. These changes may be compensatory mechanisms in the metabolically and physiologically stressed photoreceptors to maintain some synaptic transmission. Downstream of photoreceptors, horizontal and bipolar cells in P23H show increases in genes involved in axon guidance and dendritic self-avoidance, suggesting active synaptic remodeling, consistent with what is found in mammalian models with RD [83]. Future studies will have to investigate the extent to which rewiring occurs and how regeneration plays a role in maintenance of the proper circuitry. While mammalian models display reprogramming of rod bipolar cells to OFF bipolar cells through a shift in expression of receptor phenotypes (i.e., mGlur receptors to iGlur receptors), our zebrafish model did not display a complete loss of ON or rod bipolar cell phenotype. We believe the ongoing regeneration of rod photoreceptors prevents a complete reprogramming, however, the extent of reprogramming that takes place in our model must be further studied.

In the inner retina, we noted increased expression of genes involved in glutamate signaling, especially certain ionotropic glutamate receptors, in some amacrine and ganglion cell clusters of P23H compared to WT. This correlates well with enhanced spontaneous activity and oscillatory behaviors in the retina of mammalian models of retinal degeneration [18, 95] and specifically with signatures of enhanced ionotropic glutamatergic input to amacrine and ganglion cells in retinal degeneration [13, 83]. This suggests that despite the ongoing regeneration of rods, the zebrafish model of RP displays features very similar to mammalian RP models. Even with continuous regeneration, this spontaneous activity could reduce the signal-to-noise ratio and pose a problem for effective vision restoration.

The retina has an endogenous circadian clock that regulates many physiological functions within the retina including POS shedding and phagocytosis, retinomotor movements and synaptic ribbon changes. Dampening and desynchronization of circadian rhythms from zeitgebers were seen in a rat model of RP when photoreceptor degeneration was advanced [96]. Surprisingly, we see an elevated expression of certain transcripts involved in regulating the circadian rhythm in the P23H zebrafish, including *per1b*, *per2*, *cry1aa*, and *tefa* in the cones, bipolar cells and RPE. Most of these genes are transcriptional repressors and are generally expressed in the same phase of the circadian cycle [45]. The WT and P23H single-cell transcriptome libraries we used were prepared at the same time of day from animals with the same environmental light cycle. There may be a phase shift in the circadian rhythm in P23H, or perhaps wholesale disruption of the circadian rhythm. This needs to be further investigated.

Some of the elevated circadian genes are also components of the *hsf2* stress response pathway. It is possible that responses to stress in the cell types physically close to the degenerating rods drive broader changes in the circadian regulators. In the present model, we also encounter continuous photoreceptor regeneration and hence the changes may not be comparable to RP models with advanced degeneration. At late stages, the circadian rhythm might be further modified, suggesting a cascade of circadian-controlled activities in the retina are affected. It has been shown in many studies that the disruption of the circadian pattern is associated with many pathological conditions including obesity, cancer and blindness [97–99]. In this case, their circadian rhythms would be expected to exhibit a non-24-h pattern. A recent study has shown that melatonin supplementation decreased the rate of desynchronization of the circadian rhythm and improved visual function in P23H rats [100]. This provides a new possibility for treating RP through circadian synchronization and hence it is important to understand the changes in the circadian pattern in different models of RP to get a better understanding of the role of circadian rhythm on RP.

Acute damage models in zebrafish, mice, and chicks have utilized light damage and NMDA treatment to study photoreceptor and inner retinal neuron degeneration/regeneration, respectively [25]. These studies have been able to show transcriptionally how MGCs become activated as well as the regulatory networks that lead to reactive gliosis or retinal regeneration [25]. Over the course of 10-day post-acute damage in zebrafish, retinal damage is detected, MGCs are activated, regeneration ensues, and MGCs return their inactivated state [25]. While acute damage models provide great insight into regeneration, they may not appropriately represent how the retina remodels when there is a chronic genetic disease such as RP. When comparing the data from our study to Hoang et al. 2020 25, we found that the MGC population found in the P23H retina was transcriptionally comparable to the resting MGCs in the trajectory of MGC response to acute damage, indicating that regeneration may come from resident progenitor cells instead of MGCs in our chronic model. Furthermore, in the light damage models, all photoreceptors were damaged simultaneously. While we believe our model represents phases 1 and 2 of mammalian retinal degeneration, such acute damage would be classified as phase 3 due to the lack of photoreceptors. Furthermore, the loss of inner neurons through NMDA would place such an acute damage in a position to study regeneration comparable to phase 4 of mammalian retinal degeneration.

Tissue remodeling during retinal degenerative diseases stands as one of the greatest barriers to implementing regenerative or bionic therapies to restore vision [15, 101]. Our study provides a foundation to understand the molecular underpinnings of the neuronal remodeling that occurs in phases 1 and 2 of retinal degeneration and will help us to understand the steps that need to be taken for successful vision restoration. It also highlights the major changes in RPE metabolism and tight junction integrity that must be dealt with in any therapeutic strategy.

As with every single-cell study, our study has its own limitations. Tissue dissociation bias is intrinsic to the approach, making direct comparison of numbers of cells within different cell types of questionable validity. We have attempted to compare the numbers of cells within a given cell type to the same cell type in different samples, employing systematic sample handling procedures as described in the methods and repeated experiments as discussed in the results. It is important to understand that changes in relative numbers of cells within a type should be considered approximations, and changes in numbers of cell types such as RPE could reflect altered adherence of the cells to the retina during isolation. Another limitation is that the sequencing depth in each cell is relatively shallow so that it is not possible to detect the expression of a gene of interest in every cell in which it is expressed. Also, since a number of computational tools have been developed and are context-dependent, it may not be possible to strictly correlate cell type clusters identified in this study with cell types identified in other studies.

Supplementary Information The online version contains supplementary material available at https://doi.org/10.1007/s00018-023-05021-1.

Acknowledgements The authors like to thank Dr. Chai-An Mao for helpful discussions, Dr. Steven W. Wang for guidance with retinal dissociation and Dr. Yumei Li at the Baylor College of Medicine Single Cell Genomics Core for expert single-cell library preparation and sequencing services.

Author contributions Conceptualization: JO, Funding acquisition: JO, ES, Methodology: AS, ES, Investigation: AS, ES, Formal analysis: AS, ES, HW, JW, Visualization: AS, ES, Writing—original draft: AS, Writing—review and editing: AS, ES, JO, HW, JW.

Funding This work was supported by a Grant from the William Stamps Farish Fund, the Louisa Stude Sarofim endowment, facility Grant G20RR024000, core Grants P30EY028102 and P30EY007551, and the University of Houston College of Optometry. ES was supported by F31EY034793 and training Grant TL1TR003169. JW is supported by NIH Grants R01NS088353 and R21NS113068 and the Amy and Edward Knight Fund of the UTHSC Senator Lloyd Bentsen Stroke Center. Single-cell library preparation and sequencing at the Baylor College of Medicine Single Cell Genomics Core was partially supported by NIH shared instrument Grants S10OD023469 and S10OD025240, core Grant P30EY002520 and CPRIT Grant RP200504.

Data and materials availability The transgenic zebrafish strain Tg (rho:MmuRho_P23H-FLAG)^{uth4} is available for research purposes from the authors with a Material Transfer Agreement with the University of Texas Health Science Center at Houston. Data from this study can be explored at https://www.opt.uh.edu/research/zebrafish/. Raw data have been deposited in GEO under Project Numbers GSE234435 and GSE234661.

Declarations

Conflict of interests The authors declare that they have no competing financial interests.

Ethics approval All procedures employing animals comply with the U.S. Public Health Service policy on humane care and use of laboratory animals and the NRC Guide for the Care and Use of Laboratory Animals and have been reviewed and approved by the Institutional Animal Care and Use Committee at the University of Texas Health Science Center at Houston under protocols HSC-AWC-15-0057 and HSC-AWC-18-0047, and at the University of Houston under protocol PROTO202100037.

References

1. Hamel C (2006) Retinitis pigmentosa. Orphanet J Rare Dis. https://doi.org/10.1186/1750-1172-1-40
2. Parmeggiani F (2011) Clinics, epidemiology and genetics of retinitis pigmentosa. Curr Genomics 12:236–237. https://doi.org/10.2174/138920211795860080
3. Wright AF, Chakarova CF, Abd El-Aziz MM, Bhattacharya SS (2010) Photoreceptor degeneration: genetic and mechanistic dissection of a complex trait. Nat Rev Genet 11:273–284. https://doi.org/10.1038/nrg2717
4. Viringipurampeer IA, Metcalfe AL, Bashar AE, Sivak O, Yanai A, Mohammadi Z, Moritz OL, Gregory-Evans CY, Gregory-Evans K (2016) NLRP3 inflammasome activation drives bystander cone photoreceptor cell death in a P23H rhodopsin model of retinal degeneration. Hum Mol Genet 25:1501–1516
5. Campochiaro PA, Mir TA (2018) The mechanism of cone cell death in Retinitis Pigmentosa. Prog Retin Eye Res 62:24–37. https://doi.org/10.1016/j.preteyeres.2017.08.004
6. Hartong DT, Berson EL, Dryja TP (2006) Retinitis pigmentosa. The Lancet 368:1795–1809
7. Weleber RG, Pennesi ME, Wilson DJ, Kaushal S, Erker LR, Jensen L, McBride MT, Flotte TR, Humphries M, Calcedo R, Hauswirth WW, Chulay JD, Stout JT (2016) Results at 2 years after gene therapy for RPE65-deficient leber congenital amaurosis and severe early-childhood-onset retinal dystrophy. Ophthalmology 123:1606–1620. https://doi.org/10.1016/j.ophtha.2016.03.003

8. Daiger SP, Sullivan LS, Bowne SJ (2013) Genes and mutations causing retinitis pigmentosa. Clin Genet 84:132–141. https://doi.org/10.1111/cge.12203
9. MacLaren RE, Bennett J, Schwartz SD (2016) Gene therapy and stem cell transplantation in retinal disease: the new frontier. Ophthalmology 123:S98–S106. https://doi.org/10.1016/j.ophtha.2016.06.041
10. Yao K, Qiu S, Wang YV, Park SJH, Mohns EJ, Mehta B, Liu X, Chang B, Zenisek D, Crair MC, Demb JB, Chen B (2018) Restoration of vision after de novo genesis of rod photoreceptors in mammalian retinas. Nature 560:484–488. https://doi.org/10.1038/s41586-018-0425-3
11. Telias M, Nawy S, Kramer RH (2020) Degeneration-dependent retinal remodeling: looking for the molecular trigger. Front Neurosci 14:618019
12. Jones BW, Watt CB, Frederick JM, Baehr W, Chen CK, Levine EM, Milam AH, Lavail MM, Marc RE (2003) Retinal remodeling triggered by photoreceptor degenerations. J Compar Neurol 464:1–16
13. Marc RE, Jones BW, Anderson JR, Kinard K, Marshak DW, Wilson JH, Wensel T, Lucas RJ (2007) Neural reprogramming in retinal degeneration. Investig Ophthalmol Vis Sci 48:3364–3371
14. Chua J, Nivison-Smith L, Fletcher EL, Trenholm S, Awatramani GB, Kalloniatis M (2013) Early remodeling of Muller cells in the rd/rd mouse model of retinal dystrophy. J Compar Neurol 521:2439–2453. https://doi.org/10.1002/cne.23307
15. Jones BW, Pfeiffer RL, Ferrell WD, Watt CB, Marmor M, Marc RE (2016) Retinal remodeling in human retinitis pigmentosa. Exp Eye Res 150:149–165. https://doi.org/10.1016/j.exer.2016.03.018
16. Pfeiffer RL, Anderson JR, Dahal J, Garcia JC, Yang JH, Sigulinsky CL, Rapp K, Emrich DP, Watt CB, Johnstun HA, Houser AR, Marc RE, Jones BW (2020) A pathoconnectome of early neurodegeneration: network changes in retinal degeneration. Exp Eye Res 199:108196. https://doi.org/10.1016/j.exer.2020.108196
17. Napoli D, Biagioni M, Billeri F, Di Marco B, Orsini N, Novelli E, Strettoi E (2021) Retinal pigment epithelium remodeling in mouse models of retinitis pigmentosa. Int J Mol Sci. https://doi.org/10.3390/ijms22105381
18. Stasheff SF (2008) Emergence of sustained spontaneous hyperactivity and temporary preservation of OFF responses in ganglion cells of the retinal degeneration (rd1) mouse. J Neurophysiol 99:1408–1421. https://doi.org/10.1152/jn.00144.2007
19. Trenholm S, Borowska J, Zhang J, Hoggarth A, Johnson K, Barnes S, Lewis TJ, Awatramani GB (2012) Awatramani Intrinsic oscillatory activity arising within the electrically coupled AII amacrine-ON cone bipolar cell network is driven by voltage-gated Na+ channels. J Physiol 590:2501–2517. https://doi.org/10.1113/jphysiol.2011.225060
20. Toychiev AH, Ivanova E, Yee CW, Sagdullaev BT (2013) Block of gap junctions eliminates aberrant activity and restores light responses during retinal degeneration. J Neurosci 33:13972–13977. https://doi.org/10.1523/JNEUROSCI.2399-13.2013
21. Telias M, Denlinger B, Helft Z, Thornton C, Beckwith-Cohen B, Kramer RH (2019) Retinoic acid induces hyperactivity, and blocking its receptor unmasks light responses and augments vision in retinal degeneration. Neuron 102:574-586e575. https://doi.org/10.1016/j.neuron.2019.02.015
22. Macosko EZ, Basu A, Satija R, Nemesh J, Shekhar K, Goldman M, Tirosh I, Bialas AR, Kamitaki N, Martersteck EM, Trombetta JJ, Weitz DA, Sanes JR, Shalek AK, Regev A, McCarroll SA (2015) Highly parallel genome-wide expression profiling of individual cells using nanoliter droplets. Cell 161:1202–1214. https://doi.org/10.1016/j.cell.2015.05.002
23. Shekhar K, Lapan SW, Whitney IE, Tran NM, Macosko EZ, Kowalczyk M, Adiconis X, Levin JZ, Nemesh J, M. (2016) Goldman comprehensive classification of retinal bipolar neurons by single-cell transcriptomics. Cell 166:1308–1323 (**e1330**)
24. Laboissonniere LA, Martin GM, Goetz JJ, Bi R, Pope B, Weinand K, Ellson L, Fru D, Lee M, Wester AK, Liu P, Trimarchi JM (2017) Single cell transcriptome profiling of developing chick retinal cells. J Compar Neurol 525:2735–2781. https://doi.org/10.1002/cne.24241
25. Hoang T, Wang J, Boyd P, Wang F, Santiago C, Jiang L, Yoo S, Lahne M, Todd LJ, Jia M (2020) Gene regulatory networks controlling vertebrate retinal regeneration. Science. https://doi.org/10.1126/science.abb8598
26. Santhanam A, Shihabeddin E, Atkinson JA, Nguyen D, Lin YP, O'Brien J (2020)A Zebrafish model of retinitis pigmentosa shows continuous degeneration and regeneration of rod photoreceptors. Cells. https://doi.org/10.3390/cells9102242
27. Westerfield M (2000) The zebrafish book: a guide for the laboratory use of zebrafish http://zfin.org/zf_info/zfbook/zfbk.html
28. Butler A, Hoffman P, Smibert P, Papalexi E, Satija R (2018) Integrating single-cell transcriptomic data across different conditions, technologies, and species. Nat Biotechnol 36:411–420. https://doi.org/10.1038/nbt.4096
29. Bindea G, Mlecnik B, Hackl H, Charoentong P, Tosolini M, Kirilovsky A, Fridman WH, Pages F, Trajanoski Z, Galon J (2009) ClueGO: a Cytoscape plug-in to decipher functionally grouped gene ontology and pathway annotation networks. Bioinformatics 25:1091–1093. https://doi.org/10.1093/bioinformatics/btp101
30. Zhou Y, Zhou B, Pache L, Chang M, Khodabakhshi AH, Tanaseichuk O, Benner C, Chanda SK (2019) Metascape provides a biologist-oriented resource for the analysis of systems-level datasets. Nat Commun 10:1523. https://doi.org/10.1038/s41467-019-09234-6
31. Wang F, Flanagan J, Su N, Wang LC, Bui S, Nielson A, Wu X, Vo HT, Ma XJ, Luo Y (2012) RNAscope: a novel in situ RNA analysis platform for formalin-fixed, paraffin-embedded tissues. J Mol Diagn 14:22–29. https://doi.org/10.1016/j.jmoldx.2011.08.002
32. Ait-Ali N, Fridlich R, Millet-Puel G, Clerin E, Delalande F, Jaillard C, Blond F, Perrocheau L, Reichman S, Byrne LC, Olivier-Bandini A, Bellalou J, Moyse E, Bouillaud F, Nicol X, Dalkara D, van Dorsselaer A, Sahel JA, Leveillard T (2015) Rod-derived cone viability factor promotes cone survival by stimulating aerobic glycolysis. Cell 161:817–832. https://doi.org/10.1016/j.cell.2015.03.023
33. Han JYS, Kinoshita J, Bisetto S, Bell BA, Nowak RA, Peachey NS, Philip NJ (2020) Philp Role of monocarboxylate transporters in regulating metabolic homeostasis in the outer retina: Insight gained from cell-specific Bsg deletion. FASEB J 34:5401–5419. https://doi.org/10.1096/fj.201902961R
34. Jiang K, Mondal AK, Adlakha YK, Gumerson J, Aponte A, Gieser L, Kim JW, Boleda A, Brooks MJ, Nellissery J, Fox DA, Balaban R, Covian R, Swaroop A (2022) Multi-omics analyses reveal early metabolic imbalance and mitochondrial stress in neonatal photoreceptors leading to cell death in Pde6brd1/rd1 mouse model of retinal degeneration. Hum Mol Genet. https://doi.org/10.1093/hmg/ddac013
35. Hagstrom SA, North MA, Nishina PL, Berson EL, Dryja TP (1998) Recessive mutations in the gene encoding the tubby-like protein TULP1 in patients with retinitis pigmentosa. Nat Genet 18:174–176. https://doi.org/10.1038/ng0298-174
36. Dilan TL, Moye AR, Salido EM, Saravanan T, Kolandaivelu S, Goldberg AFX, Ramamurthy V (2019) ARL13B, a Joubert syndrome-associated protein, is critical for retinogenesis and elaboration of mouse photoreceptor outer segments. Neurosci

39:1347–1364. https://doi.org/10.1523/JNEUROSCI.1761-18.2018
37. Chen J, Shi G, Concepcion FA, Xie G, Oprian D, Chen J (2006) Stable rhodopsin/arrestin complex leads to retinal degeneration in a transgenic mouse model of autosomal dominant retinitis pigmentosa. J Neurosci 26:11929–11937. https://doi.org/10.1523/JNEUROSCI.3212-06.2006
38. Grossman GH, Watson RF, Pauer GJ, Bollinger K, Hagstrom SA (2011) Immunocytochemical evidence of Tulp1-dependent outer segment protein transport pathways in photoreceptor cells. Exp Eye Res 93:658–668. https://doi.org/10.1016/j.exer.2011.08.005
39. Perkins BD, Kainz PM, O'Malley DM, Dowling JE (2002) Transgenic expression of a GFP-rhodopsin COOH-terminal fusion protein in zebrafish rod photoreceptors. Vis Neurosci 19:257–264
40. Morris AC, Schroeter EH, Bilotta J, Wong RO, Fadool JM (2005) Cone survival despite rod degeneration in XOPS-mCFP transgenic zebrafish. Invest Ophthalmol Vis Sci 46:4762–4771. https://doi.org/10.1167/iovs.05-0797
41. Sun C, Galicia C, Stenkamp DL (2018) Transcripts within rod photoreceptors of the Zebrafish retina. BMC Genomics 19:1–18
42. Hirayama J, Miyamura N, Uchida Y, Asaoka Y, Honda R, Sawanobori K, Todo T, Yamamoto T, Sassone-Corsi P, Nishina H (2009) Common light signaling pathways controlling DNA repair and circadian clock entrainment in zebrafish. Cell Cycle 8:2794–2801. https://doi.org/10.4161/cc.8.17.9447
43. Petit L, Ma S, Cipi J, Cheng SY, Zieger M, Hay N, Punzo C (2018) Aerobic glycolysis is essential for normal rod function and controls secondary cone death in retinitis pigmentosa. Cell Rep 23:2629–2642. https://doi.org/10.1016/j.celrep.2018.04.111
44. Amaral IP, Johnston IA (2012) Circadian expression of clock and putative clock-controlled genes in skeletal muscle of the zebrafish. Am J Physiol Regul Integr Comp Physiol 302:R193-206. https://doi.org/10.1152/ajpregu.00367.2011
45. Weger BD, Sahinbas M, Otto GW, Mracek P, Armant O, Dolle D, Lahiri K, Vallone D, Ettwiller L, Geisler R, Foulkes NS, Dickmeis T (2011) The light responsive transcriptome of the zebrafish: function and regulation. PLoS ONE 6:e17080. https://doi.org/10.1371/journal.pone.0017080
46. Shakhmantsir I, Dooley SJ, Kishore S, Chen D, Pierce E, Bennett J, Sehgal A (2020) RNA splicing factor mutations that cause retinitis pigmentosa result in circadian dysregulation. J Biol Rhythms 35:72–83. https://doi.org/10.1177/0748730419887876
47. Feng W, Yasumura D, Matthes MT, LaVail MM, Vollrath D (2002) Mertk triggers uptake of photoreceptor outer segments during phagocytosis by cultured retinal pigment epithelial cells. J Biol Chem 277:17016–17022. https://doi.org/10.1074/jbc.M107876200
48. Chrenek MA, Dalal N, Gardner C, Grossniklaus H, Jiang Y, Boatright JH, Nickerson JM (2012) Analysis of the RPE sheet in the rd10 retinal degeneration model. Adv Exp Med Biol 723:641–647. https://doi.org/10.1007/978-1-4614-0631-0_81
49. Kokkinopoulos I, Shahabi G, Colman A, Jeffery G (2011) Mature peripheral RPE cells have an intrinsic capacity to proliferate; a potential regulatory mechanism for age-related cell loss. PLoS ONE 6:e18921. https://doi.org/10.1371/journal.pone.0018921
50. Ortolan D, Sharma R, Volkov A, Maminishkis A, Hotaling NA, Huryn LA, Cukras C, Di Marco S, Bisti S, Bharti K (2022) Single-cell–resolution map of human retinal pigment epithelium helps discover subpopulations with differential disease sensitivity. Proc Natl Acad Sci 119:e2117553119
51. Xu Z, Liao X, Li N, Zhou H, Li H, Zhang Q, Hu K, Yang P, Hou S (2021) A single-cell transcriptome atlas of the human retinal pigment epithelium. Front Cell Develop Biol 9:802457
52. Lee H, Lee H-Y, Chae J-B, Park C-W, Kim C, Ryu J-H, Jang J, Kim N, Chung H (2022) Single-cell transcriptome of the mouse retinal pigment epithelium in response to a low-dose of doxorubicin. Commun Biol 5:722
53. Senabouth A, Daniszewski M, Lidgerwood GE, Liang HH, Hernández D, Mirzaei M, Keenan SN, Zhang R, Han X, Neavin D (2022) Transcriptomic and proteomic retinal pigment epithelium signatures of age-related macular degeneration. Nat Commun 13:4233
54. Sparrow JR, Hicks D, Hamel CP (2010) The retinal pigment epithelium in health and disease. Curr Mol Med 10:802–823. https://doi.org/10.2174/156652410793937813
55. Punzo C, Xiong W, Cepko CL (2012) Loss of daylight vision in retinal degeneration: are oxidative stress and metabolic dysregulation to blame? J Biol Chem 287:1642–1648. https://doi.org/10.1074/jbc.R111.304428
56. Falasconi A, Biagioni M, Novelli E, Piano I, Gargini C, Strettoi E (2019) Retinal phenotype in the rd9 mutant mouse, a model of X-linked RP. Front Neurosci 13:991
57. Husse J, Hintze SC, Eichele G, Lehnert H, Oster H (2012) Circadian clock genes Per1 and Per2 regulate the response of metabolism-associated transcripts to sleep disruption. PLoS ONE 7:e52983. https://doi.org/10.1371/journal.pone.0052983
58. Cai J, Nelson KC, Wu M, Sternberg P Jr, Jones DP (2000) Oxidative damage and protection of the RPE. Prog Retin Eye Res 19:205–221. https://doi.org/10.1016/s1350-9462(99)00009-9
59. Rajala RV (2010) Phosphoinositide 3-kinase signaling in the vertebrate retina. J Lipid Res 51:4–22. https://doi.org/10.1194/jlr.R000232
60. Perlmann T, Jansson L (1995) A novel pathway for vitamin A signaling mediated by RXR heterodimerization with NGFI-B and NURR1. Genes Dev 9:769–782. https://doi.org/10.1101/gad.9.7.769
61. Connaughton VP, Graham D, Nelson R (2004) Identification and morphological classification of horizontal, bipolar, and amacrine cells within the zebrafish retina. J Compar Neurol 477:371–385
62. Chen CK, Wieland T, Simon MI (1996) RGS-r, a retinal specific RGS protein, binds an intermediate conformation of transducin and enhances recycling. Proc Natl Acad Sci USA 93:12885–12889. https://doi.org/10.1073/pnas.93.23.12885
63. Arshavsky VY, Pugh EN Jr (1998) Lifetime regulation of G protein-effector complex: emerging importance of RGS proteins. Neuron 20:11–14. https://doi.org/10.1016/s0896-6273(00)80430-4
64. Shintani T, Ihara M, Tani S, Sakuraba J, Sakuta H, Noda M (2009) APC2 plays an essential role in axonal projections through the regulation of microtubule stability. J Neurosci 29:11628–11640. https://doi.org/10.1523/JNEUROSCI.2394-09.2009
65. Zhou Z, Xu H, Li Y, Yang M, Zhang R, Shiraishi A, Kiyonari H, Liang X, Huang X, Wang Y, Xie Q, Liu S, Chen R, Bao L, Guo W, Wang Y, Meng W (2020) CAMSAP1 breaks the homeostatic microtubule network to instruct neuronal polarity. Proc Natl Acad Sci U S A 117:22193–22203. https://doi.org/10.1073/pnas.1913177117
66. Marc RE, Jones BW, Watt CB, Strettoi E (2003) Neural remodeling in retinal degeneration. Prog Retinal Eye Res 22:607–655
67. Cederlund ML, Morrissey ME, Baden T, Scholz D, Vendrell V, Lagnado L, Connaughton VP, Kennedy BN (2011) Zebrafish Tg(7.2mab21l2:EGFP)ucd2 transgenics reveal a unique population of retinal amacrine cells. Invest Ophthalmol Vis Sci 52:1613–1621. https://doi.org/10.1167/iovs.10-5376
68. Missler M, Sudhof TC (1998) Neurexophilins form a conserved family of neuropeptide-like glycoproteins. J Neurosci 18:3630–3638
69. Arimura N, Okada M, Taya S, Dewa KI, Tsuzuki A, Uetake H, Miyashita S, Hashizume K, Shimaoka K, Egusa S, Nishioka T, Yanagawa Y, Yamakawa K, Inoue YU, Inoue T, Kaibuchi K,

Hoshino M (2020) DSCAM regulates delamination of neurons in the developing midbrain. Sci Adv. https://doi.org/10.1126/sciadv.aba1693
70. Geng RX, Li N, Xu Y, Liu JH, Yuan FE, Sun Q, Liu BH, Chen QX (2018) Identification of core biomarkers associated with outcome in glioma: evidence from bioinformatics analysis. Dis Markers. https://doi.org/10.1155/2018/3215958
71. Tezel G, Hernandez R, Wax MB (2000) Immunostaining of heat shock proteins in the retina and optic nerve head of normal and glaucomatous eyes. Arch Ophthalmol 118:511–518. https://doi.org/10.1001/archopht.118.4.511
72. Fuhrmann S (2008) Wnt signaling in eye organogenesis. Organogenesis 4:60–67. https://doi.org/10.4161/org.4.2.5850
73. Wu S, Nguyen LTM, Pan H, Hassan S, Dai Y, Xu J, Wen Z (2020) Two phenotypically and functionally distinct microglial populations in adult zebrafish. Sci Adv. https://doi.org/10.1126/sciadv.abd1160
74. Mitchell DM, Sun C, Hunter SS, New DD, Stenkamp DL (2019) Regeneration associated transcriptional signature of retinal microglia and macrophages. Sci Rep 9:4768. https://doi.org/10.1038/s41598-019-41298-8
75. Kyritsis N, Kizil C, Zocher S, Kroehne V, Kaslin J, Freudenreich D, Iltzsche A, Brand M (2012) Acute inflammation initiates the regenerative response in the adult zebrafish brain. Science 338:1353–1356
76. Nagashima M, Hitchcock PF (2021) Inflammation regulates the multi-step process of retinal regeneration in zebrafish. Cells 10:783
77. Powell C, Cornblath E, Elsaeidi F, Wan J, Goldman D (2016) Zebrafish Müller glia-derived progenitors are multipotent, exhibit proliferative biases and regenerate excess neurons. Scientific Rep 6:1–10
78. Mercer SE, Odelberg SJ, Simon HG (2013) A dynamic spatiotemporal extracellular matrix facilitates epicardial-mediated vertebrate heart regeneration. Dev Biol 382:457–469. https://doi.org/10.1016/j.ydbio.2013.08.002
79. Ouyang X, Panetta NJ, Talbott MD, Payumo AY, Halluin C, Longaker MT, Chen JK (2017) Hyaluronic acid synthesis is required for zebrafish tail fin regeneration. PLoS ONE 12:e0171898. https://doi.org/10.1371/journal.pone.0171898
80. Minegishi Y, Nakaya N, Tomarev SI (2018) Mutation in the Zebrafish cct2 gene leads to abnormalities of cell cycle and cell death in the retina: a model of CCT2-related leber congenital amaurosis. Invest Ophthalmol Vis Sci 59:995–1004. https://doi.org/10.1167/iovs.17-22919
81. Zhao Y, Liu X, He Z, Niu X, Shi W, Ding JM, Zhang L, Yuan T, Li A, Yang W, Lu L (2016) Essential role of proteasomes in maintaining self-renewal in neural progenitor cells. Sci Rep 6:19752. https://doi.org/10.1038/srep19752
82. Jones BW, Kondo M, Terasaki H, Watt CB, Rapp K, Anderson J, Lin Y, Shaw MV, Yang JH, Marc RE (2011) Retinal remodeling in the Tg P347L rabbit, a large-eye model of retinal degeneration. J Compar Neurol 519:2713–2733
83. Pfeiffer RL, Marc RE, Jones BW (2020) Persistent remodeling and neurodegeneration in late-stage retinal degeneration. Prog Retinal Eye Res 74:100771
84. Peng Y-W, Hao Y, Petters RM, Wong F (2000) Ectopic synaptogenesis in the mammalian retina caused by rod photoreceptor-specific mutations. Nat Neurosci 3:1121–1127
85. Torten G, Fisher SK, Linberg KA, Luna G, Perkins G, Ellisman MH, Williams DS (2023) Three-dimensional ultrastructure of the normal rod photoreceptor synapse and degenerative changes induced by retinal detachment. J Neurosci 43:5468–5482
86. Lin B, Masland RH, Strettoi E (2009) Remodeling of cone photoreceptor cells after rod degeneration in rd mice. Exp Eye Res 88:589–599
87. Aranda ML, Schmidt TM (2020) Diversity of intrinsically photosensitive retinal ganglion cells: circuits and functions. Cell Mol Life Sci. https://doi.org/10.1007/s00018-020-03641-5
88. Strettoi E, Pignatelli V (2000) Modifications of retinal neurons in a mouse model of retinitis pigmentosa. Proc Natl Acad Sci 97:11020–11025
89. Stefanov A, Novelli E, Strettoi E (2020) Inner retinal preservation in the photoinducible I307N rhodopsin mutant mouse, a model of autosomal dominant retinitis pigmentosa. J Compar Neurol 528:1502–1522
90. Strettoi E, Porciatti V, Falsini B, Pignatelli V, Rossi C (2002) Morphological and functional abnormalities in the inner retina of the rd/rd mouse. J Neurosci 22:5492–5504
91. Yu DY, Cringle SJ (2005) Retinal degeneration and local oxygen metabolism. Exp Eye Res 80:745–751. https://doi.org/10.1016/j.exer.2005.01.018
92. Shi DY, Xie FZ, Zhai C, Stern JS, Liu Y, Liu SL (2009) The role of cellular oxidative stress in regulating glycolysis energy metabolism in hepatoma cells. Mol Cancer 8:32. https://doi.org/10.1186/1476-4598-8-32
93. Sinclair JW, Hoying DR, Bresciani E, Nogare DD, Needle CD, Berger A, Wu W, Bishop K, Elkahloun AG, Chitnis A, Liu P, Burgess SM (2021) The Warburg effect is necessary to promote glycosylation in the blastema during zebrafish tail regeneration. NPJ Regen Med 6:55. https://doi.org/10.1038/s41536-021-00163-x
94. Fukuda R, Marin-Juez R, El-Sammak H, Beisaw A, Ramadass R, Kuenne C, Guenther S, Konzer A, Bhagwat AM, Graumann J, Stainier DY (2020) Stimulation of glycolysis promotes cardiomyocyte proliferation after injury in adult zebrafish. EMBO Rep 21: 49752. https://doi.org/10.15252/embr.201949752
95. Trenholm S, Awatramani GB (2015) Origins of spontaneous activity in the degenerating retina. Front Cell Neurosci 9:277. https://doi.org/10.3389/fncel.2015.00277
96. Lax P, Otalora BB, Esquiva G, Rol Mde L, Madrid JA, Cuenca N (2011) Circadian dysfunction in P23H rhodopsin transgenic rats: effects of exogenous melatonin. J Pineal Res 50:183–191. https://doi.org/10.1111/j.1600-079X.2010.00827.x
97. Lockley SW, Skene DJ, Arendt J, Tabandeh H, Bird AC, Defrance R (1997) Relationship between melatonin rhythms and visual loss in the blind. J Clin Endocrinol Metab 82:3763–3770. https://doi.org/10.1210/jcem.82.11.4355
98. Savvidis C, Koutsilieris M (2012) Circadian rhythm disruption in cancer biology. Mol Med 18:1249–1260. https://doi.org/10.2119/molmed.2012.00077
99. Turek FW, Joshu C, Kohsaka A, Lin E, Ivanova G, McDearmon E, Laposky A, Losee-Olson S, Easton A, Jensen DR, Eckel RH, Takahashi JS, Bass J (2005) Obesity and metabolic syndrome in circadian Clock mutant mice. Science 308:1043–1045. https://doi.org/10.1126/science.1108750
100. Fuentes-Broto L, Perdices L, Segura F, Orduna-Hospital E, Insa-Sanchez G, Sanchez-Cano AI, Cuenca N, Pinilla I (2021) Effects of daily melatonin supplementation on visual loss, circadian rhythms, and hepatic oxidative damage in a rodent model of retinitis pigmentosa. Antioxidants (Basel). https://doi.org/10.3390/antiox10111853
101. Jones BW, Kondo M, Terasaki H, Lin Y, McCall M, Marc RE (2012) Retinal remodeling. Jpn J Ophthalmol 56:289–306. https://doi.org/10.1007/s10384-012-0147-2